Journal of Marine Systems 245 (2024) 103996

Contents lists available at ScienceDirect

Journal of Marine Systems

journal homepage: www.elsevier.com/locate/jmarsys

Investigating Labrador Sea's persistent surface O_2 anomaly using observations and biogeochemical model results

Amavi N. Silva [a,*], Duncan A. Purdie [a], Nicholas R. Bates [b,c], Toby Tyrrell [a]

[a] Ocean and Earth Science, National Oceanography Centre Southampton, University of Southampton, Southampton, UK
[b] School of Ocean Futures, School of Earth and Space Exploration and Julie Ann Wrigley Global Futures Laboratory, Arizona State University (ASU), Tempe, AZ, USA
[c] ASU-Bermuda Institute of Ocean Sciences, St. Georges, Bermuda

ARTICLE INFO

Keywords:
Oxygen
Labrador Sea
Biogeochemical models
Mixed layer depth
CORS method
Autonomous data quality

ABSTRACT

Deviations of surface ocean dissolved oxygen (O_2) from equilibrium with the atmosphere should be rectified about twenty times more quickly than deviations of dissolved carbon dioxide (CO_2). Therefore, persistent O_2 disequilibria in the Labrador Sea, while CO_2 is close to equilibrium, has been a matter of interest to many previous works. Here we investigate this phenomenon by using a novel analytical technique, the 'CORS (Carbon Dioxide and Oxygen Relative to Saturation) method', and also by using more data than was available previously. We compare observations to results from a model we developed for the Labrador Sea which combines plankton ecology with biogeochemical cycling of oxygen, carbon and nitrogen. In contrast to earlier works which mostly considered individual factors in isolation, here we used the model, together with data, to distinguish between the varying influences of several processes potentially contributing to the long-lasting O_2 undersaturation: mixed layer depth, duration of mixed layer deepening, convection, entrainment and bottom water O_2 content. Our model experiments confirm that, for the same gas exchange rate, the effects on surface O_2 concentration differ significantly among the identified drivers. Our results suggest that prolonged surface O_2 undersaturation is not always dependent on the extreme winter mixed layer depths, but rather that even moderately deep mixed layers (e.g. 300 m), when prolonged and in conjunction with continuous entrainment of oxygen-depleted deep water, can also drive persistent surface O_2 anomalies. An implication of our results is that regions in the North Atlantic with maximum winter mixed layer depths of only a few hundred metres should also show persistent surface O_2 undersaturation. We further reveal that convection in deep water formation regions produces trendlines that do not pass through the origin of a plot of CO_2 vs. O_2 deviations which have previously been thought to indicate erroneous data.

1. Introduction

Oxygen (O_2) carries a special importance in biogeochemical studies owing to its fundamental role in maintaining life on earth and regulating nutrient and carbon cycles. Dissolved concentrations of O_2 [O_2] in the global ocean are a reflection of the balance between air-sea gas exchange, biological fluxes (i.e. organic matter production and remineralization) and physical fluxes (i.e. cooling, warming, deep convection, upwelling). O_2 is slightly supersaturated almost everywhere in the surface ocean (Sarmiento and Gruber, 2006) due to O_2 production via photosynthesis. Respiration below the mixed layer reduces O_2 concentrations below solubility equilibrium, creating oxygen minimum zones (Wyrtki, 1962). The slow thermohaline circulation causes O_2 to ventilate the deep global ocean, ensuring survival and existence of aerobic marine life forms in nearly all bottom waters. Climate models predict that increased emissions of greenhouse gases would weaken the thermohaline circulation and impact deep-ocean ventilation (Manabe and Stouffer, 1993; Matear et al., 2000; Wood et al., 1999), eventually resulting in vertical expansion of oxygen minimum zones in tropical waters (Bograd et al., 2008; Stramma et al., 2008; Whitney et al., 2007) which may dramatically alter marine ecosystem structures. Boyer et al. (2013) estimated that the global ocean's oxygen inventory is equal to 200 Pmol O_2. Schmidtko et al. (2017) recently found that deep ocean O_2 inventory has been declining by approx. 700 Tmol decade^{-1} since the 1960s.

O_2 equilibration in the ocean-atmosphere system is brought about by

* Corresponding author.
E-mail address: dans1m19@soton.ac.uk (A.N. Silva).

https://doi.org/10.1016/j.jmarsys.2024.103996
Received 16 January 2024; Received in revised form 17 May 2024; Accepted 3 June 2024
Available online 4 June 2024

gas exchange which acts to restore surface ocean oxygen concentrations towards equilibrium with the atmosphere (Keeling et al., 1998). Given that O_2 only dissolves in the ocean and is not reactive with seawater, unlike carbon dioxide (CO_2) which undergoes equilibria reactions to form carbonic acid (H_2CO_3), carbonate (CO_3^{2-}) and bicarbonate (HCO_3^-), the surface ocean is predicted to be kept close to O_2 saturation continuously through rapid air-sea gas exchange (Oschlies et al., 2018). Hence, following a perturbation, such as caused by a bloom of phytoplankton, it is expected that O_2 returns to its equilibrium approximately twenty times faster than CO_2 (Sarmiento and Gruber, 2006; Zeebe and Wolf-Gladrow, 2001), leading to ephemeral O_2 disequilibria while CO_2 disequilibria remain persistent. Vachon et al. (2020), from a study of the two gases in lakes, state that '*measurements of O_2 and CO_2 concentration often show decoupling over diel and longer time scales*'. In line with this argument, results from a simplified model to investigate how surface ocean O_2 and dissolved inorganic carbon (DIC) concentrations (in a 40 m deep surface mixed layer of constant temperature, salinity and alkalinity; a detailed model description is given in supplementary information) predicted to change following a phytoplankton bloom find that in the presence of air-sea gas exchange, the *e*-folding time for O_2 to recover towards equilibrium (for 66.7% of a perturbation to be removed) is 13 days, whereas for CO_2 it is 3 months (Fig. 1).

The distribution of O_2 disequilibrium in the surface global ocean has been investigated previously by several studies, focusing on regional and temporal trends and forcing factors. Broecker and Peng (1982) and Najjar and Keeling (1997) showed that the global ocean maintains long-term surface O_2 equilibrium with the atmosphere. Conkright et al. (2002) and Sarmiento and Gruber (2006) noted, from data compilations, a near ubiquitous slight O_2 supersaturation globally, with $[O_2]$ nearly always close to and usually slightly above the temperature-related solubility value. Observations by Carrillo et al. (2004) in waters off West Antarctic Peninsula, Emerson (1987) and Emerson and Stump (2010) in the Subarctic Pacific Ocean, and Tortell et al. (2014) in coastal Antarctic waters showed oxygen's ability to recover from a perturbation within several weeks. Craig and Hayward (1987) and Giomi et al. (2019) noted the prevalent slight O_2 supersaturation in the tropical and subtropical oceans, and the importance of biological fluxes in bringing this about. Nevertheless, the understanding above suggests that surface O_2 should return to saturation quickly after a perturbation, compared to CO_2, and therefore we should expect to often see CO_2 disequilibria in the absence of O_2 disequilibria.

A new perspective was provided by Wu et al. (2022) when they plotted O_2-CO_2 deviations from the atmospheric equilibrium in the global surface ocean and found coupled deviations to be more common than uncoupled deviations. The frequency of substantial deviations of $[O_2]$ from the saturation value is surprising in light of the foregoing, and seems in need of explanation. O_2 undersaturation can be brought about either by a decrease in in-situ $[O_2]$ or by an increase in O_2 solubility. Several earlier studies (e.g. Bushinsky et al., 2017; Duteil et al., 2013; Gordon and Huber, 1990; Körtzinger et al., 2004; Russell and Dickson, 2003) have suggested possible mechanisms capable of producing O_2 undersaturation through the following: (1) increased solubility due to heat loss and subsequent cooling; (2) entrainment of O_2-poor deep water into the surface waters and, (3) seasonal sea ice-cover preventing air-sea gas exchange from restoring the surface ocean to saturation. These mechanisms have the potential to produce persistent surface O_2 undersaturation in polar and subpolar oceans, thus shedding light on the findings of Wu et al. (2022).

The Labrador Sea, a semi-enclosed sea in the Subpolar North Atlantic basin, is one such oceanographic region which exhibits long duration undersaturation of surface O_2 (Clarke and Coote, 1988; Körtzinger et al., 2008); it has therefore been the focus of many oceanographic studies over the past years. The Labrador Sea is one of the few areas in the global ocean where O_2 from the atmosphere can directly reach the deep ocean, hence, ventilating the intermediate and deep waters of the North Atlantic basin (Koelling et al., 2022; Rhein et al., 2017). It is characterised by deep water convection reaching to depths between 700 and 2300 m during winter which results in the formation of Labrador Sea Water, a significant contributor to the formation of North Atlantic Deep Water (Avsic et al., 2006; Kieke and Yashayaev, 2015; Lazier, 1973; Marshall and Schott, 1999; Yashayaev, 2007). The time taken for the Labrador Sea's mixed layer to deepen and the maximum depth it reaches are determined by the severity of winter each year (Curry et al., 1998; Pickart et al., 2002; Schulze et al., 2016). Supporting this, studies by Bacon et al. (2003), Centurioni and Gould (2004) and de Jong et al. (2012) discussed the importance of mixed layers over convective mixing in deep water formation regions. Density based mixed layer depth (hereafter known as 'MLD') maps derived by Kara et al. (2003) show that, in general, the maximum MLD in the deep water formation regions are the greatest anywhere in the global ocean.

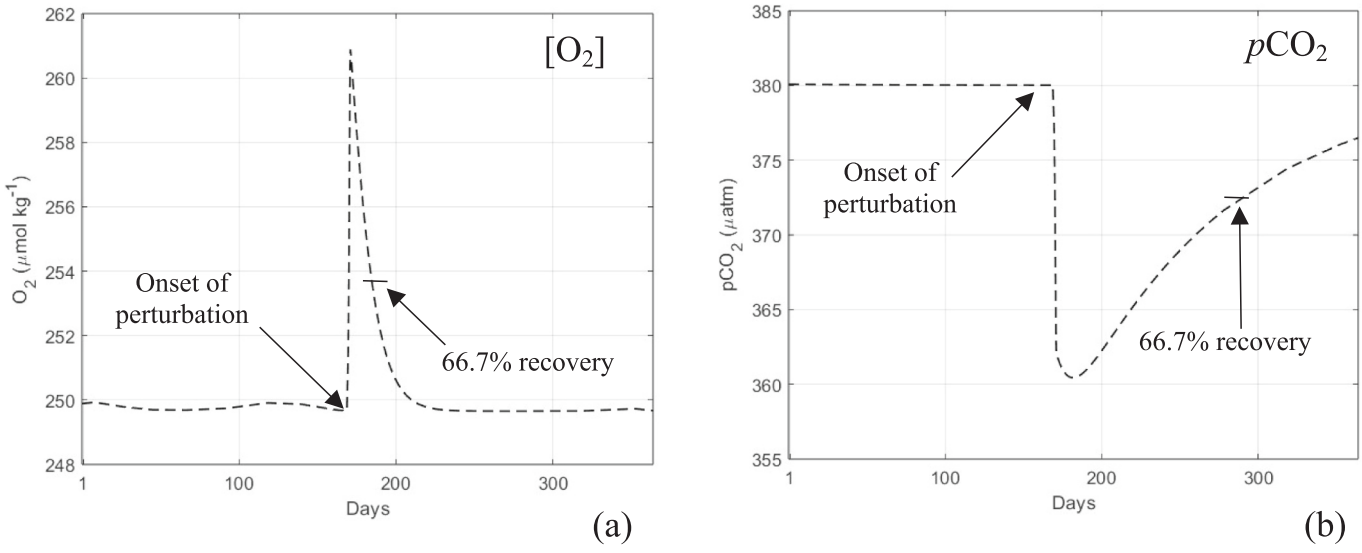

Fig. 1. Behaviour of surface $[O_2]$ and pCO_2 over a period of one year. To produce this figure, the model used in this study was simplified so that the only environmental driver affecting the system would be air-sea gas exchange (all other processes, such as entrainment and mixing were excluded). $[O_2]$ and pCO_2 were perturbed away from the equilibrium at day 169, by adding photosynthesis and remineralization to the model for a period of 50 days, in order to observe how the system responds to a phytoplankton bloom in the presence of air-sea gas exchange. (a) Evolution of surface O_2 concentration. (b) Evolution of surface pCO_2 content.

When the Labrador Sea's winter mixed layer loses its buoyancy and deepens, extending to great depths, the consequent incorporation of deep water into the deepening mixed layer drives a strong ocean-atmosphere O_2 gradient (Atamanchuk et al., 2020; Koelling et al., 2017; Koelling et al., 2022; Wolf et al., 2018). When the mixed layer stays very deep for months, the resulting convection carries O_2-poor bottom waters to the surface at rates too rapid to be balanced by air-sea gas exchange which eventually leads to a persistent surface O_2 under-saturation in the Labrador Sea waters (Clarke and Coote, 1988; Koelling et al., 2017; Koelling et al., 2022; Körtzinger et al., 2008; Wolf et al., 2018). This extremely deep convection of the Labrador Sea leads to strong nutrient replenishment subsequently fuelling intense phyto-plankton blooms during summer (Frajka-Williams and Rhines, 2010; Head et al., 2000; Longhurst, 2007). Due to thermohaline stratification of the Labrador Sea, these blooms occur in the mixed layer, driving near-surface O_2 levels towards supersaturation (Frajka-Williams et al., 2009; Wu et al., 2008). Therefore, significant seasonality in these physical (i.e. heat, wind, convection) and biological (i.e. organic matter production and remineralization) processes make the Labrador Sea an interesting region to study for its dynamic yet persistent surface O_2 disequilibria.

Körtzinger et al. (2008) studied full surface seasonal cycles of both O_2 and CO_2 in the region using a mooring station time series and concluded that the Labrador Sea shifts from a prolonged surface O_2 undersaturation of 6% during winter to a short O_2 supersaturation of 10% during summer, making the region act as a net O_2 sink. O_2 is thus pushed away from saturation for the majority of its annual cycle, with air-sea gas exchange able to bring about equilibrium only for a period of 30 days. Wolf et al. (2018) used Argo float-derived data to estimate that

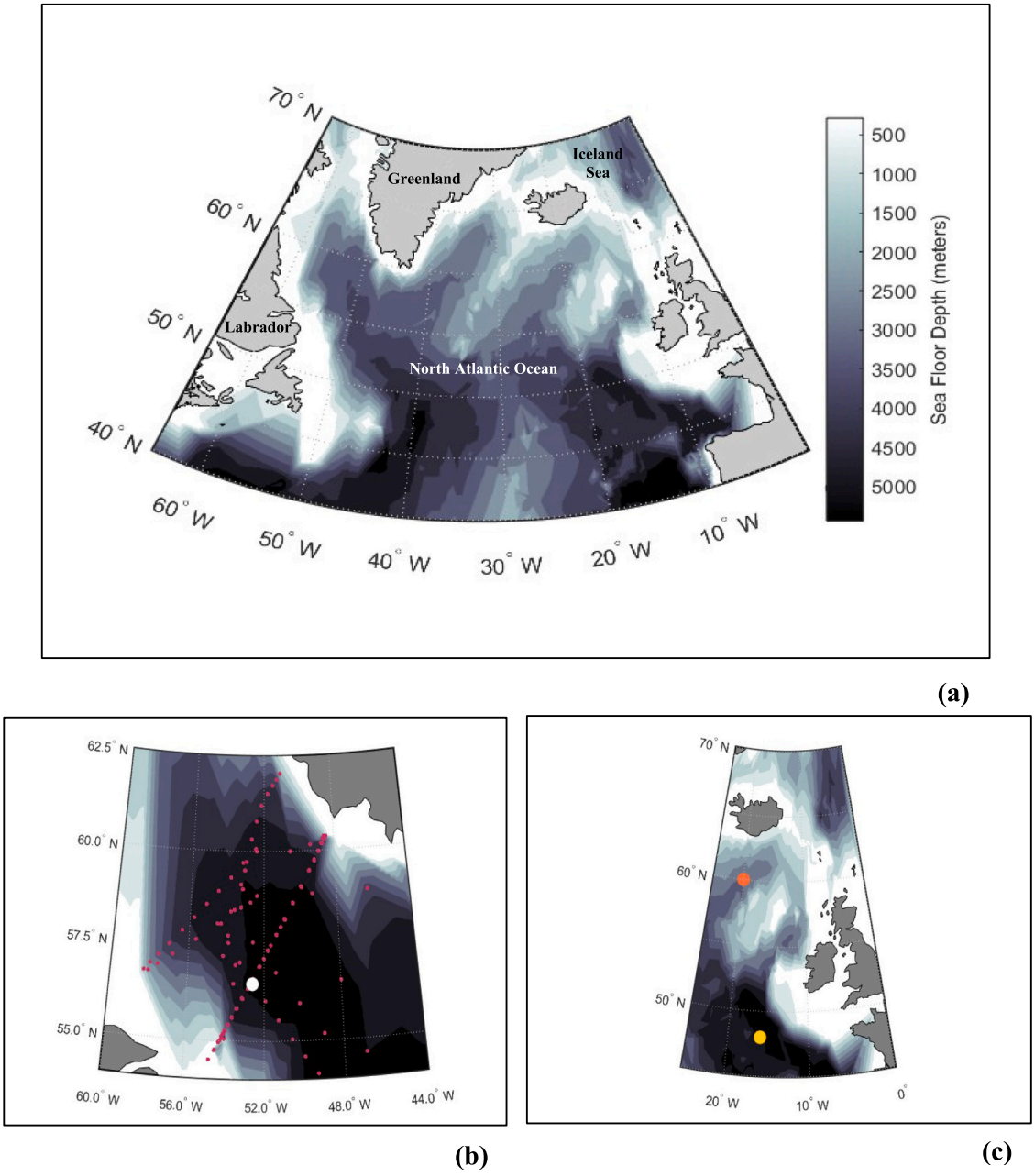

Fig. 2. Study sites and sampling locations. (a) The location of the Labrador Sea in the North Atlantic Ocean basin. (b) Sampling locations from where K1 data (white circle) and GLODAPv2 data (red points) were taken. (c) Locations in the south of Iceland (amber circle) and Porcupine Abyssal Plain (yellow circle) from where NCEP/NCAR reanalysis MLD results were taken. (For interpretation of the references to colour in this figure legend, the reader is referred to the web version of this article.)

at the end of convection, O_2 in the Labrador Sea reaches an undersaturation of 6.1% to 7.6%. An earlier model study by Clarke and Coote (1988) demonstrated that the saturation state of the wintertime surface O_2 is constrained by the region's MLD. According to Koelling et al. (2022) and McKinley et al. (2003), this O_2 disequilibrium causes intense uptake of atmospheric O_2 in the Labrador Sea which in turn ventilates the Labrador Sea Waters and contributes significantly in 'quenching' the O_2 'thirst' in the deep Atlantic Ocean.

In this paper, we revisit the Labrador Sea's O_2 anomaly using a novel analytical approach: the 'CORS (Carbon dioxide and Oxygen Relative to Saturation) method'. Devised by Wu et al. (2022), this technique compares concentrations of O_2 and CO_2 with the atmospheric equilibrium as well as with each other, and identifies possible bio-physical drivers responsible for the deviations. Here, the CORS method is applied to mooring data and quality controlled ship-board measurements. In addition, we present a newly developed coupled ecosystem-biogeochemical model that studies O_2 and CO_2 cycles of the region and their constraints. The main aim of this work was to use model simulations, informed by data, to examine the relative importance of different physical and biological processes in producing the region's months-long surface O_2 undersaturation.

2. Method

2.1. Data sources

The primary data source in this study was data from the K1 site (hereafter referred to as 'K1') in the Central Labrador Sea (Figs. 2a and b), an oceanographic mooring site (56.5°N, 52.6°W) in the subpolar region of the Northwest Atlantic Ocean (the dataset was obtained upon request from GEOMAR: Helmholtz-Centre for Ocean Research, Kiel). The K1 site has been in operation since 1996, for the fundamental purpose of studying deep convection trends of the region (Avsic et al., 2006; Lavender et al., 2002). Sensors deployed at different depths between 38 m and 798 m were used to measure physical and chemical properties with a temporal resolution between 15 min and 2 h (DeGrandpre et al., 1995; Körtzinger et al., 2005; Tengberg et al., 2006). For this study, the main variables we used were the quality-controlled [O_2] and the partial pressure of CO_2 (pCO_2) measurements for the period of September 2004 to July 2005, together with sea surface temperature (SST) and sea surface salinity (SSS) data, within a mixed layer that was on average 38 m deep. Oxygen Optode 3830 (Aanderaa Data Instruments) and SAMI-CO_2 (Sunburst Sensors LLC) were used to measure O_2 and pCO_2, respectively. SST and SSS measurements were made with SBE-37 MicroCAT recorders (Sea-Bird Electronics Inc.). Given that the mooring was a subsurface floatation platform instead of a surface buoy, the measurements closely reflect the surface mixed layer properties of the region (Körtzinger et al., 2008).

A major drawback of using the K1 dataset for our analyses was its lack of nutrient and deep water measurements. Surface nutrient data is important for understanding the effects of biological processes. Measurements from deeper in the water column reveal physical processes such as deep-water convection and upwelling which are generally marked by inputs of water with high nutrients, low O_2 and high CO_2. Therefore, to compensate the absence of these data in the K1 data, we also used a secondary data source: the GLODAPv2_2023 data product (hereafter known as 'GLODAPv2') of the Global Ocean Data Analysis Project (https://glodap.info/index.php/merged-and-adjusted-data-product-v2-2023/). With surface-to-bottom ocean biogeochemical data collected during the period 1973–2022 on >900 scientific cruises covering all the major ocean basins in the world, GLODAPv2 contains quality-controlled bottle measurements of O_2, DIC, Alkalinity (TA), temperature, salinity and nutrients (Lauvset et al., 2022; Olsen et al., 2020). For this study, cruise data points in the region 54°N – 64°N and 46°W – 66°W were used (Fig. 2b) with the 'surface ocean' defined as waters shallower than 30 m (Wu et al., 2022). To calculate the deep-water characteristics of the Labrador Sea, data from between 700 and 1300 m depth were used as this was the maximum thickness of the wintertime MLD identified for 2004 and 2005 during which the K1 measurements were collected (Avsic et al., 2006).

Monthly MLD values for the Labrador Sea (hereafter known as 'MLD_{LS}') were obtained from Fig. 2 of Körtzinger et al. (2008) which gives the MLD of the K1 site from September 2004 to August 2005, estimated from Argo float profiles. To compare with the MLD_{LS}, monthly MLDs of Porcupine Abyssal Plain (hereafter known as 'MLD_{PAP}') and south of Iceland (hereafter known as 'MLD_{SI}') were obtained using monthly mean ocean mixed layer depth below sea surface results from the NCEP/NCAR Reanalysis Project (Kistler et al., 2001: https://psl.noaa.gov/data/gridded/data.ncep.reanalysis.surface.html). The locations of MLD_{SI} (60°N, 20°W) and MLD_{PAP} (48°N, 16°W) are given in Fig. 2c. Annual MLD patterns observed for the three locations are presented in Fig. 3.

2.2. Surface O_2 and CO_2 deviations

Deviations of O_2 and CO_2 from atmospheric equilibrium (hereafter known as 'ΔO_2' and 'ΔCO_2', respectively) were computed using the following two equations:

$$\Delta O_2 = [O_{2obs}] - [O_{2sat}] \quad (1)$$

$$\Delta CO_2 = [CO_{2obs}] - [CO_{2sat}] \quad (2)$$

All the concentrations are expressed in μmol kg^{-1}. The subscripts 'obs' and 'sat' stand for observed concentrations and saturated concentrations (when net air-sea gas exchange is zero), respectively. [O_{2obs}] was directly extracted from the K1 and the GLODAPv2 datasets since their O_2 measurements were given as concentrations. [O_{2sat}] was calculated using the O_2 solubility equation of Garcia and Gordon (1992, 1993), modified to account for in-situ sea level pressure, using daily sea level pressure calculated from the NCEP/NCAR Reanalysis Project, as described by Wu et al. (2022). Although the effect of bubble-mediated gas exchange was not accounted for in the [O_{2sat}] calculations, we acknowledge that bubbles can also contribute to O_2 disequilibrium (Sarmiento and Gruber, 2006).

[CO_{2obs}] for the K1 dataset was calculated using the Henry's Law Equation:

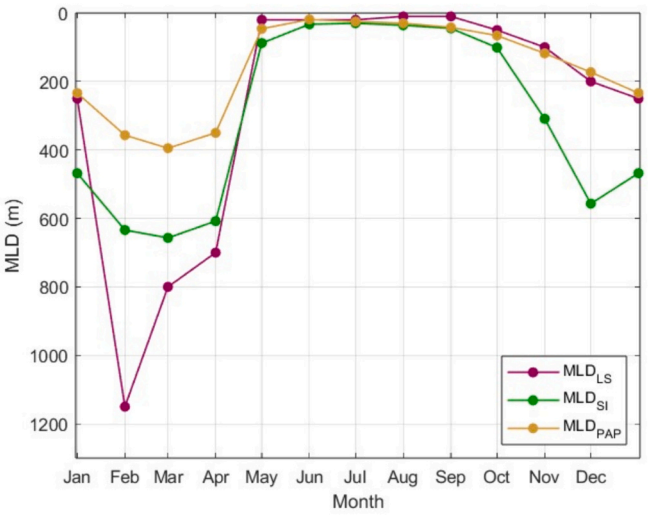

Fig. 3. Monthly MLD variability for 2004–2005 annual cycle in the Labrador Sea (purple line), south of Iceland (green line) and Porcupine Abyssal Plain (yellow line). MLD_{LS} was obtained from Körtzinger et al. (2008); MLD_{SI} and MLD_{PAP} values were obtained from the NCEP/NCAR Reanalysis Project. (For interpretation of the references to colour in this figure legend, the reader is referred to the web version of this article.)

$$[CO_{2obs}] = K_H \times pCO_{2obs} \quad (3)$$

K_H is the solubility constant of CO_2 at a given temperature and salinity, computed using the equation proposed by Weiss (1974). Surface pCO_{2obs} was directly extracted from the K1 data. $[CO_{2sat}]$ was also calculated based on Eq. 3 (modified as $[CO_{2sat}] = K_H \times$ atmospheric pCO_2 in equilibrium with seawater pCO_2). To calculate atmospheric pCO_2, the equations proposed by Takahashi et al. (2009) with average atmospheric mole fraction of CO_2 in dry air (hereafter known as 'xCO_2' which is equal to 378.8 ppm for the year 2004/5), in-situ sea level pressure, and the water vapour pressure (calculated from in-situ humidity data as proposed by Weiss and Price, 1980) were used.

Since the GLODAPv2 data do not have pCO_2 measurements, both surface and bottom $[CO_{2obs}]$ values were calculated using the Matlab version of the CO2SYS v1.1 calculator (van Heuven et al., 2011) with in-situ DIC, TA, temperature, salinity, phosphate and silicate data as inputs. $[CO_{2sat}]$ values were also estimated based on Eq. 3 where globally averaged surface annual mean xCO_2 data (published in https://www.esrl.noaa.gov/gmd/ccgg/trends/) was used to calculate annual atmospheric pCO_2 values for each corresponding sampling year. The dissociation constants for carbonic acid and sulphate were taken from Lueker et al. (2000) and Dickson (1990) respectively.

2.3. ΔCO_2 vs. ΔO_2 on a 'CORS' plot

Calculated ΔO_2 and ΔCO_2 values were used to construct a CORS plot, the primary output of the CORS method. A CORS plot is a scatter plot with the x-axis representing ΔO_2 and the y-axis, ΔCO_2. The two axes intersect at the origin (0,0), dividing the CORS plot into four quadrants. Quadrant 1 indicates a signal of $\Delta O_2 > 0$ and $\Delta CO_2 > 0$, implying simultaneous supersaturation of the two gases which could be driven by surface warming or sea ice formation events. Quadrant 2 is characterised by $\Delta O_2 < 0$ and $\Delta CO_2 > 0$, i.e. O_2 undersaturation coupled with CO_2 supersaturation that could be caused by organic matter remineralization, deep water convection and/or upwelling. Quadrant 3 is marked by a signal of simultaneous undersaturation of O_2 and CO_2 ($\Delta O_2 < 0$ and $\Delta CO_2 < 0$) which could be the result of surface cooling or ice melting events. Quadrant 4 corresponds to an anti-correlated pattern for O_2 and CO_2 with the former being supersaturated ($\Delta O_2 > 0$) and the latter undersaturated ($\Delta CO_2 < 0$), the typical signal of organic matter production. When the large majority of points in a dataset are at or near to the origin of the CORS plot, then this indicates that the system is usually close to equilibrium with regards to O_2 and CO_2, i.e. that air-sea gas exchange dominates. When ΔO_2 and ΔCO_2 are decoupled (when one gas is at saturation while the other is pushed away), the points in a CORS plot will be aligned along the axis which represents the deviated gas. These 'signal – driver(s)' relationships were described previously by Wu et al. (2022).

2.4. Monthly changes of ΔO_2 and ΔCO_2

The monthly changes to ΔO_2 and ΔCO_2 were calculated using average monthly ΔO_2 and ΔCO_2 values, using the following equation:

$$\Delta X_{chg} = \Delta X_{(n)} - \Delta X_{(n-1)} \quad (4)$$

'X' is either O_2 or CO_2 and 'n' is the month number. For example, if $n = 5$, then this indicates the month of May; 'n-1' represents the month of April. Thus, when average ΔO_2 for April is -24 μmol kg^{-1} and average ΔO_2 for May is -0.4 μmol kg^{-1}, ΔO_{2chg} of May (from April) would be 23.6 μmol kg^{-1} (Table 1).

2.5. Expected trends for biological drivers

In order to re-analyse the role of biological drivers in the Labrador Sea as identified by previous work, we computed predicted photosynthetic and deep-water respiration effects using GLODAPv2 data.

Table 1
Month to month ΔO_2 and ΔCO_2 changes (ΔO_{2chg} and ΔCO_{2chg}) in the Labrador Sea. The changes were calculated as differences between adjacent monthly averages (given by Eq. 4 in the main text). '+' and '-' symbols indicate 'increase' and 'decrease', respectively. ΔO_{2chg} and ΔCO_{2chg} for September was calculated from July due to the absence of August data (Hence ΔO_{2chg} and ΔCO_{2chg} for September indicate changes of concentrations since the month before previous).

Month	Average ΔO_2 (μmol kg^{-1})	ΔO_{2chg} (μmol kg^{-1})	Average ΔCO_2 (μmol kg^{-1})	ΔCO_{2chg} (μmol kg^{-1})
May	−0.4	+24	−2.0	−1.8
June	+11	+11	−3.9	−1.9
July	−1	−12	−3.1	+0.8
September	−4	−3	−3.0	+0.1
October	−5	−1	−2.5	+0.5
November	−11	−6	−1.9	+0.6
December	−16	−5	−1.4	+0.5
January	−25	−9	−0.7	+0.7
February	−27	−2	+0.1	+0.8
March	−22	+5	−0.2	−0.3
April	−24	−2	−0.2	0.0

Considering the Redfield ratio of DIC/O_2 (equivalent to 117/170; Anderson and Sarmiento, 1994), corresponding changes of DIC when $[O_2]$ is changed by ±25, ±50, ±75, ±100 μmol kg^{-1} were calculated. For example, during photosynthesis a 25 μmol kg^{-1} increase in O_2 should be accompanied by a corresponding 17.2 μmol kg^{-1} decrease in DIC. Initial DIC and $[CO_2]$ were calculated using average SSS, SST, TA and atmospheric pCO_2. Applying the calculated changes of DIC to the initial DIC concentration, final DIC and $[CO_2]$ values corresponding to O_2 changes were calculated. The changes of $[CO_2]$ (the difference between initial $[CO_2]$ and final $[CO_2]$) with respect to the changes of $[O_2]$ were then used to build up predicted photosynthesis and respiration curves on a CORS plot. For example, when SSS is 34, SST is 3.7 °C, surface TA is 2268 μmol kg^{-1}, initial DIC is 2128.7 μmol kg^{-1}, initial $[CO_2]$ is 20.8 μmol kg^{-1} and initial pCO_2 is 380 μatm, a 25 μmol kg^{-1} increase of $[O_2]$ would lead to a corresponding $[CO_2]$ decrease of 2.3 μmol kg^{-1}. Similarly, the expected respiration curve for the Labrador Sea deep water, was produced by assuming that water leaves the surface with ΔCO_2 and $\Delta O_2 = 0$ μmol kg^{-1} and then has DIC progressively added and O_2 removed in Redfield ratio proportions.

2.6. Biogeochemical model for the Labrador Sea

A coupled ecosystem-biogeochemical model was developed (hereafter known as 'LSM') to further investigate the persistent surface O_2 undersaturation of the Labrador Sea, by adapting the models proposed by Taylor et al. (1991) and Tyrrell and Taylor (1995). The LSM consists of a system with a single species of phytoplankton and a single nutrient (nitrogen) in a surface mixed layer (P_M and N_M, respectively) with a seasonally varying depth of H_M (forced by MLD_{LS}) and a thermocline directly below with a fixed thickness of H_T (40 m). Phytoplankton and nutrient concentrations (expressed in mg Chl-a m^{-3} and μmol NO_3^- kg^{-1}, respectively) in the mixed layer are denoted by P_M and N_M and those in the thermocline by P_T and N_T. In addition, a bottom layer with fixed concentrations of phytoplankton (P_B) and nutrient (N_B) was also imposed where $P_B < P_T < P_M$ and $N_B > N_T > N_M$. The model runs showed that the system exhibits a repeatable annual cycle from the second year onwards. Therefore, the LSM results of the third year were used for this study.

The following model equations show the functions describing the relationships among the above mentioned variables. Fig. 4 is a schematic diagram of the variables, processes, and parameters involved in the model. The subscripts '$_M$', '$_T$' and '$_B$' stand for the mixed layer, the thermocline and the bottom layer, respectively. A description of the model parameters along with their units and values is given in Table A1. The parameterizations and numerical methods used to develop the model eqs. (5) to (14) are given in Taylor et al. (1991) and Tyrrell and

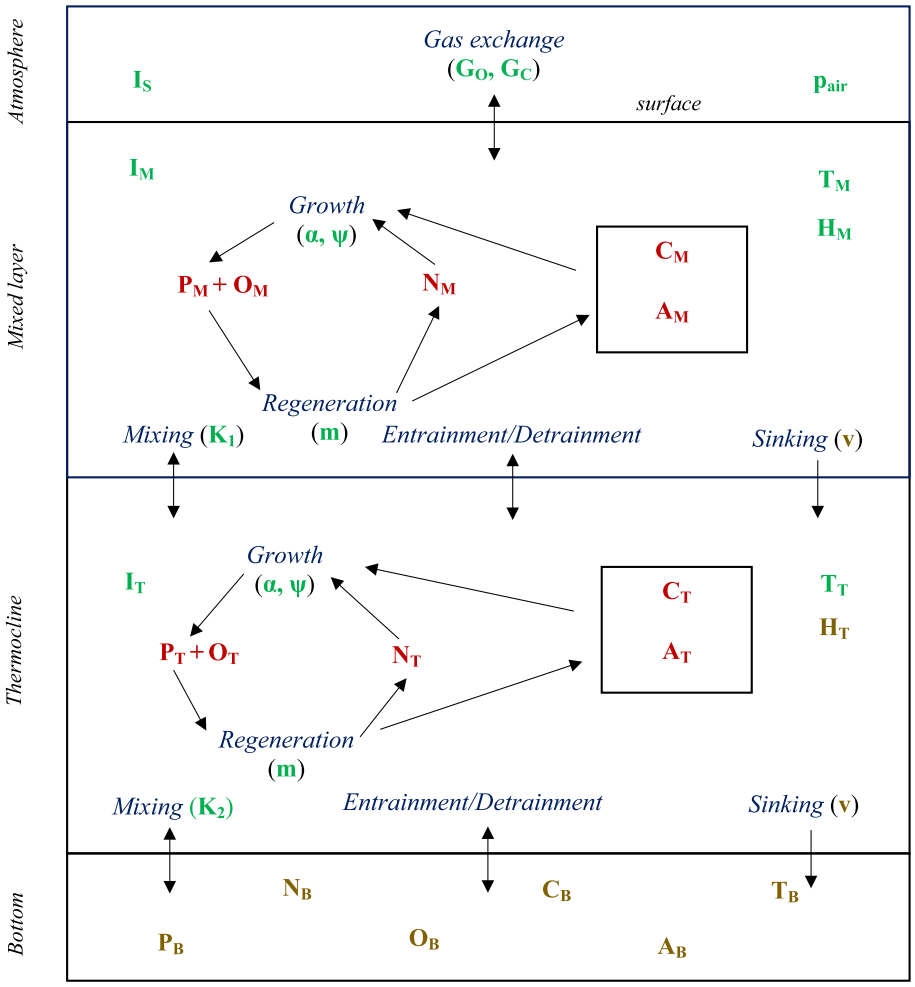

Fig. 4. Schematic diagram explaining interactions among variables and processes of the model. P, N, O, C and A are state variables (shown in red) representing phytoplankton, nutrient, O_2, DIC and TA, respectively. Processes that connect them are given in blue. Subscripts '$_S$', '$_M$', '$_T$' and '$_B$' describe the surface, the mixed layer, the thermocline and the bottom layer, respectively. Model parameters with constant values are given in brown whereas those with varying values (dependent on other factors) are given in green. All the model parameters and their values are listed in Table A1. (For interpretation of the references to colour in this figure legend, the reader is referred to the web version of this article.)

Taylor (1995).

$$dP_M/dt = P_M\,[(\alpha_M\varphi_M) - m - (v/H_M)\,] + [k_2(P_T - P_M)/H_M\,] \quad (5)$$

$$dP_T/dt = P_T\,[(\alpha_T\varphi_T) - m\,] - [(P_T - P_M)(v/H_T)\,] + [k_1(P_B - P_T)/H_T - k_2(P_T - P_M)/H_T\,] \quad (6)$$

$$dN_M/dt = -\gamma P_M\,[(\alpha_M\varphi_M) - \varepsilon m\,] + [k_2(N_T - N_M)/H_M\,] \quad (7)$$

$$dN_T/dt = -\gamma P_T\,[(\alpha_T\varphi_T) - \varepsilon m\,] + [k_1(N_B - N_T)/H_T - k_2(N_T - N_M)/H_T] \quad (8)$$

Variability in TA and DIC (both expressed in μmol kg^{-1}) were used to explain how total carbon content in the LSM is affected by phytoplankton growth and decay. A_M and C_M are the mixed layer concentrations while A_T and C_T are the thermocline concentrations. A_B and C_B, the fixed concentrations below the thermocline, were forced from the average deep TA (2300 μmol kg^{-1}) and DIC (2155 μmol kg^{-1}) values for the Labrador Sea, calculated from the GLODAPv2 data. The interactions between these state variables are shown below:

$$dA_M/dt = -\tau_A\gamma P_M\,[(\alpha_M\varphi_M) - \varepsilon m\,] + [k_2(A_T - A_M)/H_M\,] \quad (9)$$

$$dA_T/dt = -\gamma P_T\,[(\alpha_T\varphi_T) - \varepsilon m\,] + [k_1(A_B - A_T)/H_T - k_2(A_T - A_M)/H_T] \quad (10)$$

$$dC_M/dt = -P_M\,[(\tau_C\alpha_M\varphi_M) - \tau_C^{*}\varepsilon_C m\,] + [k_2(C_T - C_M)/H_M\,] + [K_{CO2}\,(p_{air} - p_m)/H_M\,] \quad (11)$$

$$dA_T/dt = -P_T\,[(\tau_C\alpha_T\varphi_T) - \tau_C^{*}\varepsilon_C m\,] + [k_1(C_B - C_T)/H_T - k_2(C_T - C_M)/H_T] \quad (12)$$

The relationships of the functions that determine the balance of the dissolved O_2 concentrations (expressed in μmol kg^{-1}) in the mixed layer (O_M) and the thermocline (O_T) are given by eqs. (13) and (14). Average deep O_2 concentration in the Labrador Sea, calculated from the GLODAPv2 data, was used to force the bottom O_2 content (O_B = 290 μmol kg^{-1}).

$$dO_M/dt = \tau_C P_M\,[(q\alpha_M\varphi_M) - \varepsilon_C m\,] + [k_2(O_T - O_M)/H_M\,] + [G_O\,(O_{sat} - O_M)/H_M\,] \quad (13)$$

$$dO_T/dt = \tau_C P_T\,[(q\alpha_T\varphi_T) - \varepsilon_C m\,] + [k_1(O_B - O_T)/H_T - k_2(O_T - O_M)/H_T\,] \quad (14)$$

Several studies show the significant role of bubbles on air-sea gas exchange across turbulent ocean surfaces (Blomquist et al., 2017; Hamme and Severinghaus, 2007; Hamme et al., 2017; Seltzer et al., 2023). Bubbles have a bigger effect on gas transfer properties of less soluble gases like O_2 than more soluble gases like CO_2 (Keeling, 1993; Memery and Merlivat, 1985; Woolf and Thorpe, 1991; Woolf et al.,

2007). Supporting these arguments, Atamanchuk et al. (2020) and Koelling et al. (2017) showed that the bubble-mediated gas transfer is a non-negligible flux component in the Labrador Sea's wintertime O_2 gas exchange, due to the region's high-wind conditions. Atamanchuk et al. (2020) also suggest that the incorporation of the bubble-effect into global models can eliminate possible underestimations to O_2 uptake in deep water formation regions. Therefore, we applied a 'bubble inclusive' flux component (F_b) to our model, calculating 'U_s', the wind speed above the sea surface in m s^{-1}, following the equation proposed by Ito et al. (2011):

When $U_s > 2.27$ m s^{-1},

$$F_b = V_b \times [(P_{atm} x O_2)/RT] \times [(U_s - 2.27)/(U_0 - 2.27)]^3 \quad (15)$$

When $U_s < 2.27$ m s^{-1}, $F_b = 0$.

U_0 is the reference wind speed (10 m s^{-1}). 'P_{atm}', 'R', and 'T_M' are sea level pressure (N m^{-2}), universal gas constant (8.31 Jmol^{-1} K^{-1}) and in-situ SST (K), respectively. The empirically determined wind speed which initiates bubble-mediated gas transfer by forming white caps is 2.27 m s^{-1}, as suggested by Monahan and Torgersen (1991). 'V_b' is a coefficient proportional to the volume of air bubbles per unit area at U_0 and empirically determined to be 9.1×10^{-9} m s^{-1} by Ito et al. (2011). 'xO_2' is the atmospheric mixing ratio of O_2 (0.21). NCEP/NCAR Reanalysis results of daily average wind speed for September 2004 – August 2005 (at the sigma 0.995 level; pressure altitude at 99.5% of the surface air pressure) were used for U_s.

A set of equations that describe the effect of entrainment and detrainment on the mixed layer and thermocline concentrations were also applied in the model. They were developed based on the fact that when the mixed layer depth increases (entrainment), each layer will gain water (together with its dissolved constituents) from the layer below and the thermocline will lose water to the mixed layer above. When the mixed layer depth shoals (detrainment) only the concentrations in the thermocline change with water being left behind in the bottom layer and water being gained from the mixed layer. Thus, when the change in the mixed layer is 'ΔH_M' and the change in the concentration of any given variable is 'ΔY', the following equations explain the effects of entrainment and detrainment in the mixed layer and the thermocline:

When $\Delta H_M > 0$ (mixed layer getting deeper),

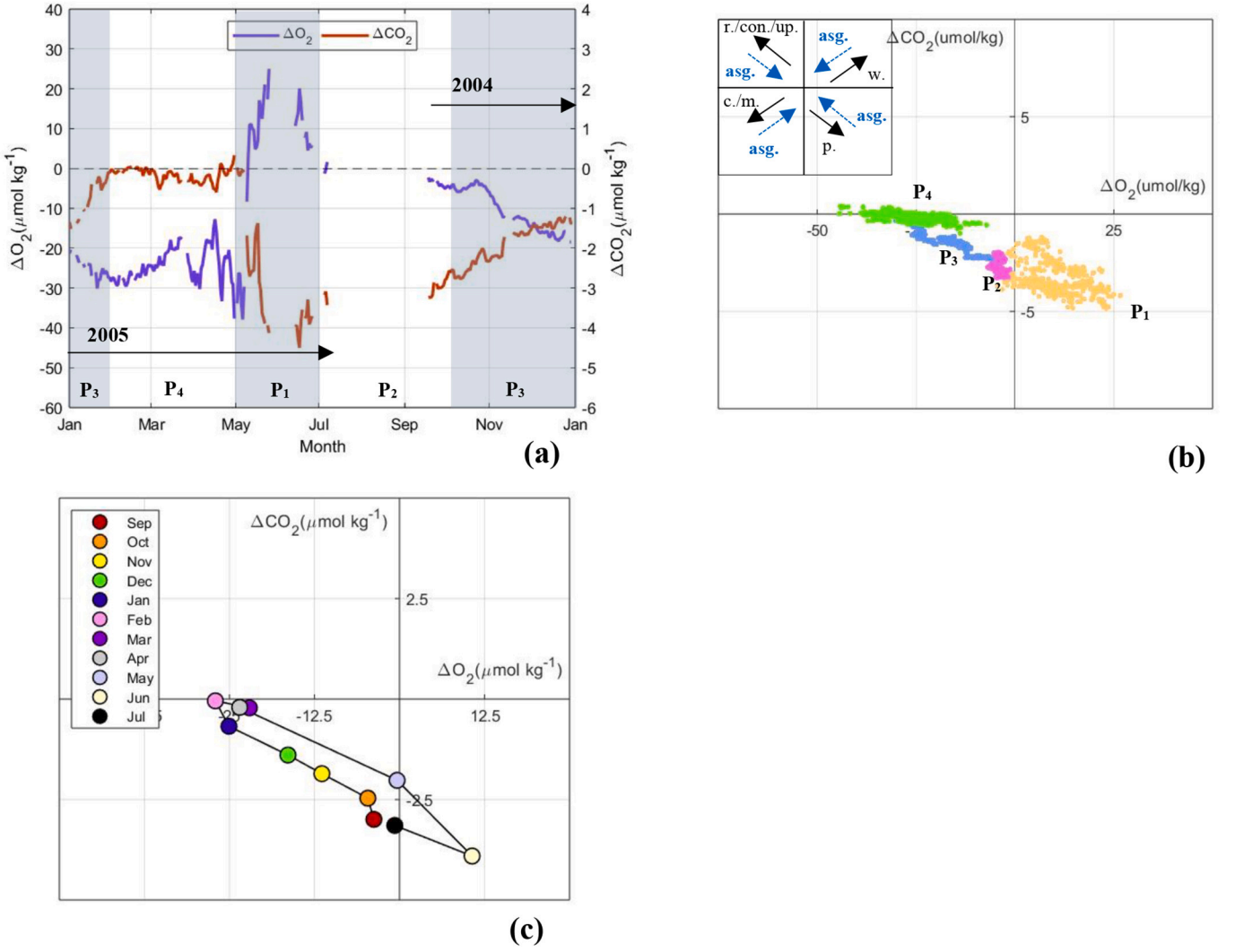

Fig. 5. Deviations of surface [O_2] and [CO_2] in the Labrador Sea for the period of September 2004 – July 2005, calculated from K1 data (Supplementary Fig. 1). (a) Time series plot showing seasonality of ΔO_2 (blue line) and ΔCO_2 (red line) for the studied year. The black dashed line shows the value at saturation (when net gas exchange is zero). Shaded and unshaded sections indicate the periods P_1 and P_3 and, P_2 and P_4, respectively. CORS plots presenting variability of ΔO_2 against ΔCO_2 of all data (b) and by monthly average (c). The insert in (b) shows the expected trends on CORS plots from major oceanic processes. 'asg.', 'w.', 'r.', 'c.', 'm.', 'con.', 'up.' and 'p.' stand for 'air-sea gas exchange', 'warming', 'respiration', 'cooling', 'melting', 'convection', 'upwelling' and 'photosynthesis', respectively. (For interpretation of the references to colour in this figure legend, the reader is referred to the web version of this article.)

$$\Delta Y_M = [(Y_M H_M + Y_T \Delta H_M)/(H_M + \Delta H_M)] - Y_M \quad (16)$$

$$\Delta Y_T = [(Y_T H_T - Y_T \Delta H_M + Y_B \Delta H_M)/H_T] - Y_T \quad (17)$$

When $\Delta H_M < 0$ (mixed layer getting shallower),

$$\Delta Y_M = 0 \quad (18)$$

$$\Delta Y_T = [(Y_T H_T - Y_T \Delta H_M + Y_M \Delta H_M)/H_T] - Y_T \quad (19)$$

3. Results

3.1. Observed O_2 against CO_2

Based on the annual cycles of surface O_2 and CO_2 in the Labrador Sea for the 2004–2005 period (Supplementary Fig. 1), we developed a time series plot (Fig. 5a), and two CORS plots (Fig. 5b: all data points; Fig. 5c: monthly averages); they show coupled ΔO_2-ΔCO_2 patterns for the surface Labrador Sea, identifying four distinctive co-variations over the studied cycle: (1) $\Delta O_2 > 0$ when $\Delta CO_2 < 0$ from May to July (hereafter referred to as 'P_1'), (2) $\Delta O_2 \sim 0$ when $\Delta CO_2 < 0$ from July to October (hereafter referred to as 'P_2'), (3) ΔO_2 and $\Delta CO_2 < 0$ from October to February (hereafter referred to as 'P_3'), and (4) $\Delta O_2 < 0$ when $\Delta CO_2 \sim 0$ from February to May (hereafter referred to as 'P_4').

Table 1 presents monthly ΔO_{2chg} and ΔCO_{2chg} in the region over the studied year. June is marked by maximum average ΔO_2 (+11 μmol kg^1) when average ΔCO_2 (−3.9 μmol kg^{-1}) is minimum. Although ΔO_2 declines to −1 μmol kg^{-1} by July, according to our results, the net ΔO_{2chg} for the P_1 period (May, June and July) is recorded to be +23 μmol kg^{-1}.

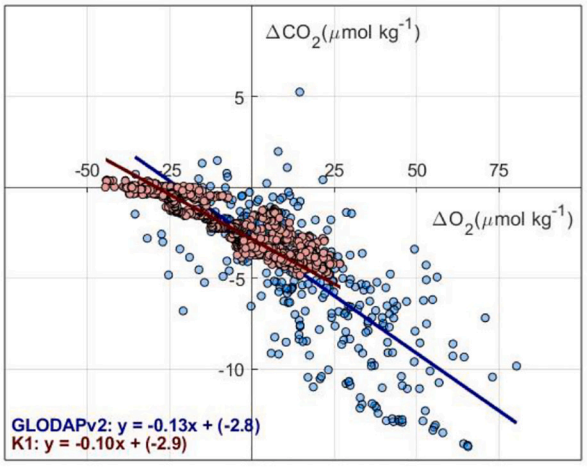

(a)

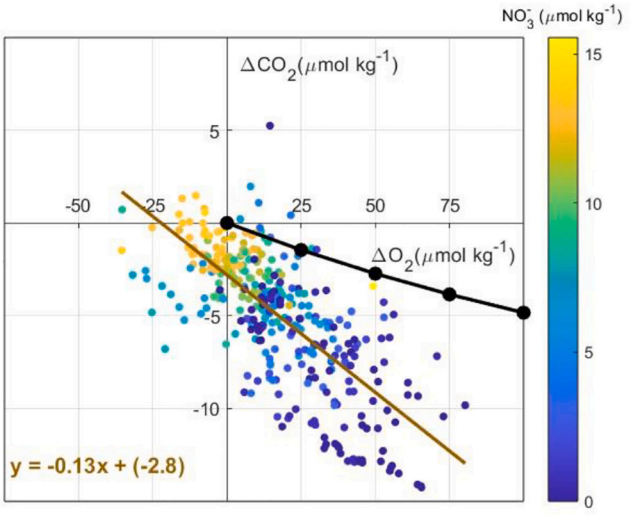

(b)

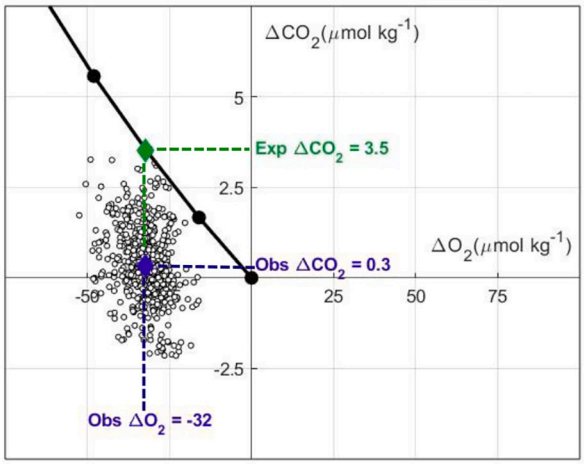

(c)

Fig. 6. ΔO_2-ΔCO_2 variability of the Labrador Sea calculated from GLODAPv2 data. (a) CORS plot showing a comparison of ΔO_2-ΔCO_2 distribution patterns in surface waters for GLODAPv2 (blue) and K1 (red) datasets. Best-fit straight lines and line equations are given in blue (for GLODAPv2) and red (for K1). (b) CORS plot for surface GLODAPv2 data where datapoints are colour-coded according to surface nitrate concentrations. The best-fit line and line equation (in brown) are same as those in (a) (shown in blue) whereas the black curve indicates the predicted photosynthetic trajectory as explained in Section 2.5. (c) CORS plot of deep water GLODAPv2 data, for the convection depth range of 700–1300 m (open circles). Black curve is the predicted deep water respiration behaviour for the dataset as explained in Section 2.5. Blue diamond shows the average observed deep water composition (ΔCO_2 = +0.3 μmol kg^{-1} and ΔO_2 = −32 μmol kg^{-1}). Green diamond shows the expected deep water ΔCO_2 (+3.5 μmol kg^{-1} due to deep water respiration) for the observed average deep water ΔO_2. (For interpretation of the references to colour in this figure legend, the reader is referred to the web version of this article.)

From September onwards O_2 slowly starts declining over the course of the next five months, while CO_2 gradually starts increasing. February marks the minimum average ΔO_2 (-27 μmol kg^{-1}) with a maximum value of 0.1 μmol kg^{-1} for near-saturated ΔCO_2. Before the large increase of ΔO_2 observed from April to May, cumulative ΔO_{2chg} for the P_3 and P_4 periods when surface O_2 shows prolonged undersaturation is calculated to be -20 μmol kg^{-1}. Cumulative ΔCO_{2chg} from the beginning of P_1 to the end of P_3 when surface CO_2 is undersaturated is -0.5 μmol kg^{-1}.

Comparison of the K1 and the GLODAPv2 data on a CORS plot (Fig. 6a) reveals that the two distributions overlap (slopes: -0.10 and -0.13 and, y-intercepts: -2.9 and -2.8, respectively), although the latter shows more spread (due to its inter-annual and spatial variability). Hence, based on the overlapping data distributions, it is reasonable to assume that it is valid to use the GLODAPv2 data to help further investigate the K1 data. Following this, Fig. 6b shows a comparison between the observed CORS pattern for the surface GLODAPv2 data, coloured by nitrate concentrations, together with its statistically estimated best-fit regression line (brown; same as shown in Fig. 6a) to the region's expected photosynthetic trajectory (black line; calculated as explained in Section 2.5). The average surface nitrate concentration of ~6.0 μmol kg^{-1} in GLODAPv2 data for the Labrador aligns well with the findings of Garcia et al. (2019) for the World Ocean Atlas 2018 where surface nitrate concentrations of the North Atlantic basin were estimated to be in the range of 0–10 μmol kg^{-1}. Moreover, a comparison between the region's expected photosynthetic curve (black) and the observed GLODAPv2-derived best-fit line (brown) shows a significant difference; the expected curve is developed by assuming that before the onset of photosynthesis the waters are saturated with O_2 and CO_2. Therefore, its y-intercept, which quantifies the value of ΔCO_2 when $\Delta O_2 = 0$, has a value of zero. In contrast, the observed curve has an anomalously negative y-intercept value of -2.8 ($\Delta CO_2 = -2.8$ μmol kg^{-1} when $\Delta O_2 = 0$).

Fig. 6c shows the deep water CORS signal in the Labrador Sea at the convection depths of 700–1300 m, with the coordinates of the blue diamond calculated by averaging GLODAPv2 data from that depth

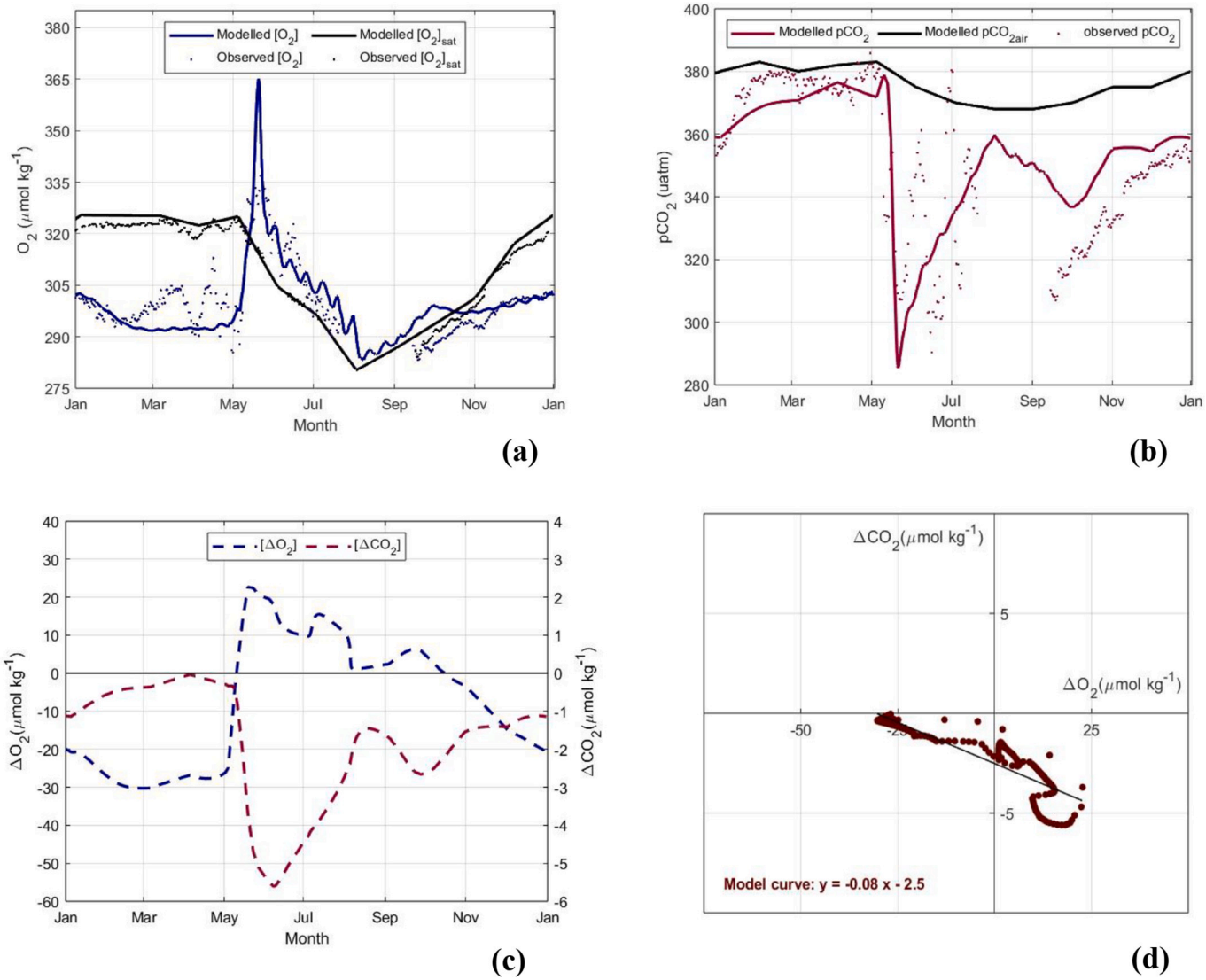

Fig. 7. Results from the coupled ecosystem-biogeochemical model (LSM) for the Labrador Sea. Predicted vs. measured (a) [O_2] and (b) pCO_2 over a span of one year. Blue points in (a) are surface [O_{2obs}] measurements (from the K1 data) and the blue curve shows mixed layer [O_2] values (O_M) from the model. Red points in (b) are observed pCO_2 (from the K1 data) while the red curve shows modelled pCO_2 (p_m). Black dots in (a) are [O_{2sat}] derived from the K1 observations. Black lines represent modelled results for (a) saturated [O_2] (O_{sat}) and (b) atmospheric pCO_2 (p_{air}). (c) Annual ΔO_2 and ΔCO_2 variability from the simulations and (d) CORS plot from the model results, together with best-fit straight line and line equation. (For interpretation of the references to colour in this figure legend, the reader is referred to the web version of this article.)

interval. The deep water CORS plot reveals a conspicuous lack of correlation between its ΔO_2 and ΔCO_2 values, an observation not further explored in this manuscript. The estimated averages for deep water ΔO_2 and ΔCO_2 values (as indicated by the blue diamond) are -32 μmol kg^{-1} and $+0.3$ μmol kg^{-1}, respectively. The black curve indicates the predicted respiration curve of the region, calculated as explained in Section 2.5. The estimated average deep water ΔCO_2 value ($+0.3$ μmol kg^{-1}) was compared against (1) the average surface ΔCO_2 value during P_4 period (-0.3 μmol kg^{-1}; Table 1) and (2) the corresponding ΔCO_2 value on the predicted respiration curve (Fig. 6c; black curve) when ΔO_2 equals to -32 μmol kg^{-1} ($+3.5$ μmol kg^{-1}; as indicated by the green diamond). The first comparison reveals that the average ΔCO_2 values for the deep and the wintertime surface of the Labrador Sea are similar in magnitude whereas the second comparison demonstrates that for the same ΔO_2 value, the deep water ΔCO_2 in the Labrador Sea shows a deficit of ~3 μmol kg^{-1}. In addition, the ranges of the deep water ΔO_2 values (between -15 μmol kg^{-1} and -50 μmol kg^{-1}) and surface water wintertime ΔO_2 values (between -10 μmol kg^{-1} and -45 μmol kg^{-1}; Fig. 5b) also exhibit close agreement.

3.2. Predicted O_2 and CO_2 trends

Fig. 7 shows the model results for the annual O_2 and pCO_2 cycles in the surface Labrador Sea. The highest $[O_2]$ peak in the model run is at 365 μmol kg^{-1} during summer, while $[O_2]$ from late winter to late spring (January to April) is nearly constant at a value of 292 μmol kg^{-1} (Fig. 7a). According to the K1 data, the summer $[O_2]$ peak is lower (340 μmol kg^{-1}) with wintertime $[O_2]$ fluctuating within a range of ~290–305 μmol kg^{-1}, until the next bloom event. $[O_{2sat}]$ values from the model and the data are in agreement (325 μmol kg^{-1}). Model pCO_2 reaches a minimum of 286 μatm in May, whereas the lowest pCO_2 in the K1 data is recorded in June (290 μatm; Fig. 7b). In-situ pCO_2 measurements in the region reveal a sudden CO_2 supersaturation (380 μatm) in July, which the model fails to replicate fully, exhibiting a peak of 360 μatm in August. From early winter to late spring (November to April), pCO_2 is observed to increase from 330 μatm to 380 μatm (saturation) and then remains at this value. The LSM also behaves similarly in this period.

A time series plot (Fig. 7c) shows the model-calculated surface ΔO_2-ΔCO_2 variability for the Labrador Sea. According to the LSM, there is a maximum O_2 supersaturation of $+23$ μmol kg^{-1} and maximum O_2 undersaturation of -30 μmol kg^{-1}, which compares to the observed values (Fig. 5a) of $+25$ μmol kg^{-1} and -38 μmol kg^{-1}, respectively. The LSM produces a maximum CO_2 undersaturation of -6 μmol kg^{-1} and a peak very close to saturation (-0.06 μmol kg^{-1}) while the values from the observed data are -5 μmol kg^{-1} and $+0.3$ μmol kg^{-1}, respectively.

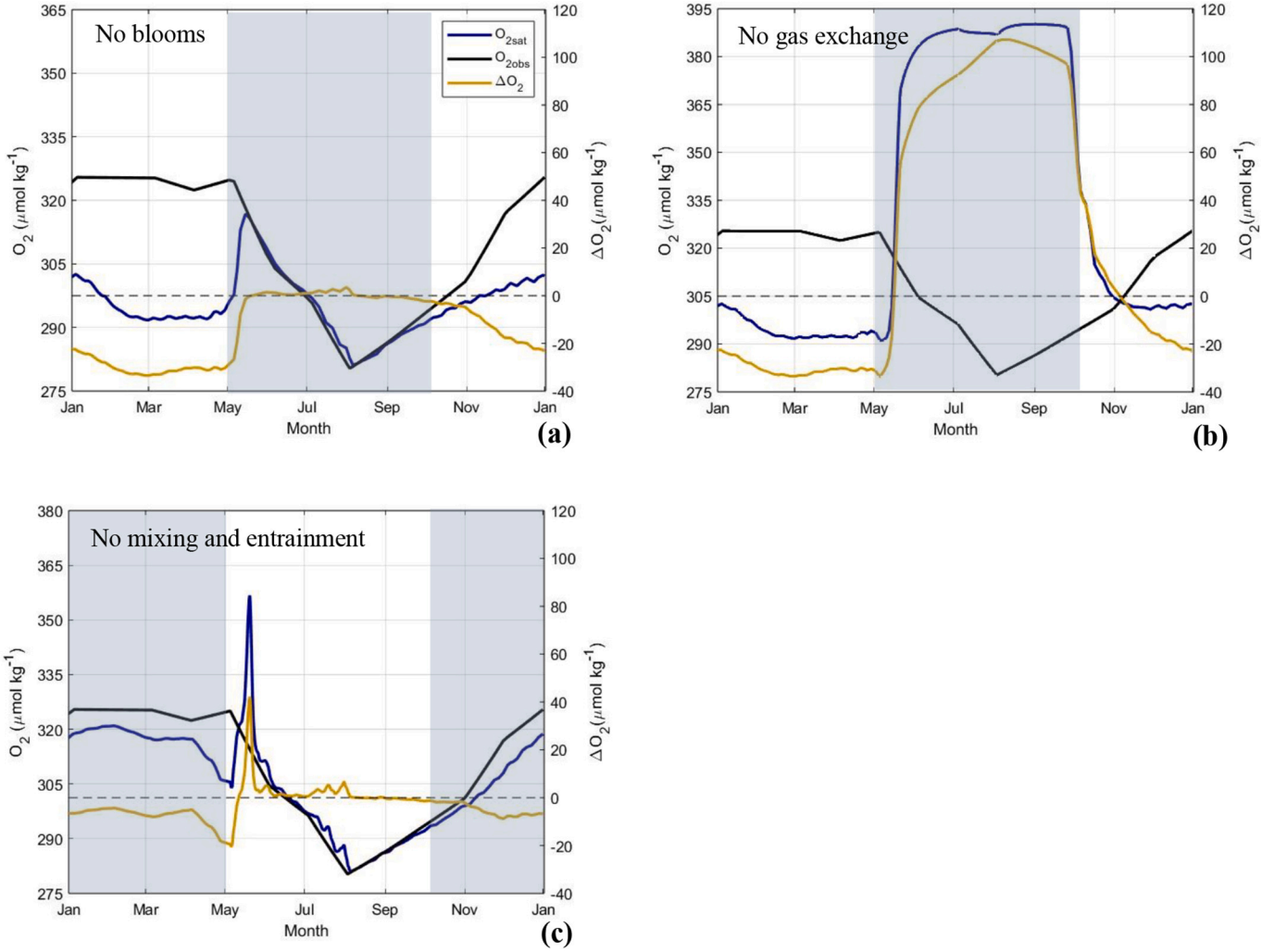

Fig. 8. Model results showing seasonality of surface $[O_2]$ (blue line) and ΔO_2 (yellow line) after the removal of each major process. Seasonality in surface $[O_2]$ and ΔO_2 when the effects of (a) biology and (b) air-sea gas exchange are absent from May to October and, (c) when the effects of deep mixing and entrainment/detrainment are absent from October to May. Shaded areas indicate the periods when each driver is absent. The black dashed line indicates $\Delta O_2 = 0$ (at saturation). (For interpretation of the references to colour in this figure legend, the reader is referred to the web version of this article.)

The slope (−0.08) and the y-intercept (−2.5) of the CORS plot from model results (Fig. 7d) compare well with those from the K1 data (−0.10 and −2.9, respectively). Model simulated O_2 and CO_2 results are strongly correlated with the K1 observations ($r = 0.93$; Supplementary Fig. 2).

3.3. Interactions among model processes

The three panels in Fig. 8 show the changes in model $[O_2]$ (blue line) and corresponding ΔO_2 (yellow line) behaviour when air-sea gas exchange, deep water mixing and bloom-driven biology are each individually excluded from the Labrador Sea for defined time periods (based on P_1 to P_4). These results should be compared to the results of the full model with no processes omitted (Fig. 7a). Removal of photosynthesis and remineralization from May to October (P_1 and P_2) pulls the $[O_2]$ curve towards the $[O_{2sat}]$ curve where it is held for the entire period (Fig. 8a) during which the corresponding ΔO_2 curve tracks the $\Delta O_2 = 0$ line (dashed black). When air-sea gas exchange is absent instead, $[O_2]$ is pushed to an extreme level of supersaturation which exceeds 380 μmol kg^{-1}, as shown by the ΔO_2 curve, and the gas does not return to equilibrium until the missing driver is restored in October (Fig. 8b). When deep water mixing and entrainment are no longer allowed to act on the region from October to May (P_3 and P_4), $[O_2]$ stays within ~10 μmol kg^{-1} of saturation (Fig. 8c).

Fig. 9 shows results from a final set of model experiments. The model's H_M (MLD) and O_B (bottom water $[O_2]$) were changed in order to investigate their influences over the wintertime surface O_2 of the Labrador Sea. The corresponding ΔO_2 variability of each experiment is given in Supplementary Fig. 3. According to Fig. 9a, when O_B = 290 μmol kg^{-1} (observed deep water $[O_2]$ for the Labrador Sea) and the LSM is forced with shallower MLD_{SI} (max. 657 m) and MLD_{PAP} (max. 395 m) instead, it causes average wintertime surface $[O_2]$ to be at 294 μmol kg^{-1} and 297 μmol kg^{-1}, respectively, only slightly higher than for deeper MLD_{LS} (max. 1150 m) at 292 μmol kg^{-1}. However, when the MLD was restricted to a maximum depth of 50 m (hereafter referred to as '$MLD_{shallow}$'), average wintertime $[O_2]$ reaches to 319 μmol kg^{-1} which is only ~6 μmol kg^{-1} away from saturation. Moreover, when the MLD was kept static (fixed at 10 m) for the annual cycle (hereafter referred to as 'MLD_{fixed}'), $[O_2]$ curve tracks the $[O_{2sat}]$ curve from October to April. On the other hand, Figs. 9b, c, and d show that when the O_B was increased in 10 μmol kg^{-1} intervals until it reaches 320 μmol kg^{-1} (thermocline O_2 content: O_T), the degree of O_2 surface undersaturation is progressively reduced in all of the runs with different winter mixed layers (MLD_{LS}, MLD_{SI} and MLD_{PAP}). Hence, in all of the runs with altered

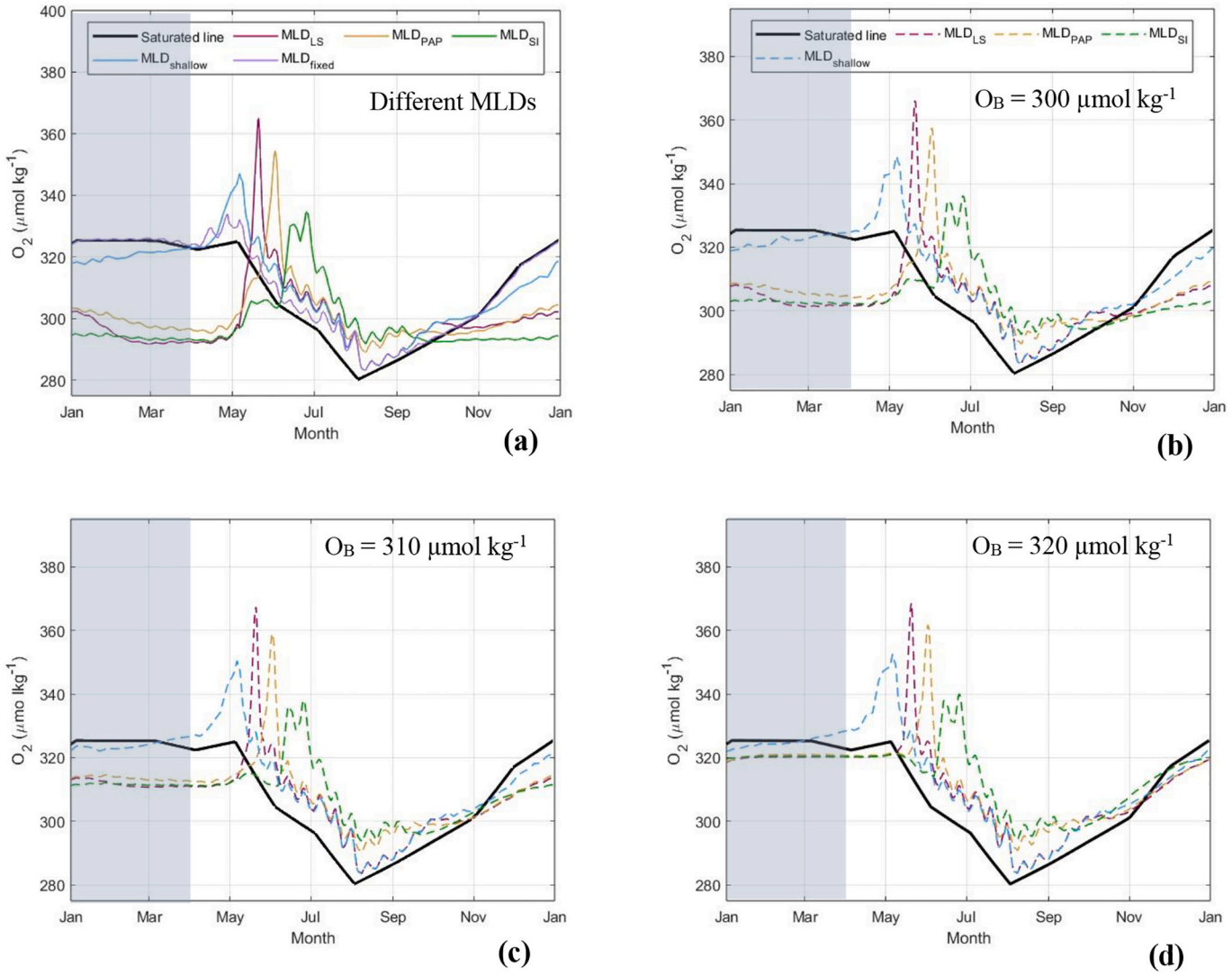

Fig. 9. Model results showing seasonality of surface $[O_2]$ under different MLDs and deep O_2 concentrations. (a) $[O_2]$ responses to the model being forced with five different MLD seasonal patterns (Fig. 3). (b), (c) and (d): $[O_2]$ responses under different MLDs when O_B is made equal to (b) 300 μmol kg^{-1}, (c) 310 μmol kg^{-1} and (d) 320 μmol kg^{-1}. The black thick line in the four subfigures indicates the $[O_2]$ saturation curve. Shaded areas indicate the period of interest.

O_B, similar patterns of winter [O_2] are obtained for MLD_{LS}, MLD_{SI} and MLD_{PAP} regardless of their maximum winter mixed layer depths. In support of this, annual surface ΔO_2 cycles investigated for the PAP and the SI using GLODAPv2 data also suggest months' long wintertime O_2 undersaturation for those regions (Fig. 10).

4. Discussion

4.1. Insights from the novel analytical approach (CORS)

One of the novel aspects of this paper is revisiting the Labrador Sea's surface O_2 deviations using the CORS method. Although a number of previous studies examined the trends of Labrador Sea's O_2 (as presented in Section 1 and later explained in detail) and CO_2 (later mentioned) separately, our work is the first to adopt an analytical approach in which the Labrador Sea's O_2 and CO_2 behaviour are analysed in a coupled way and their deviations from saturation are compared to each other. Furthermore, the CORS findings of this study shed light on O_2 and CO_2 data quality assessment which will be discussed separately in Section 4.4.

Annual O_2-CO_2 cycles of the Labrador Sea are marked by two distinctive periods when surface O_2 is pushed away from atmospheric equilibrium along with surface CO_2 (Fig. 5). During the P_1 period, spring/summer phytoplankton blooms in the area result in a strong O_2 supersaturation in early summer, which is quickly restored within less than three months, thus ensuring an ephemeral disequilibrium (as expected, according to Fig. 1a). A simultaneously occurring CO_2 deviation prevails even after O_2 atmospheric equilibrium is fully restored (as expected, according to Fig. 1b). Low surface nitrate concentrations during this period (Fig. 6b), which are associated with nutrient utilization by primary producers, further confirm this biological impact. Also, it is evident in our results that the Labrador Sea spring blooms are a highly significant driver for the region; their onset causes about 30% and 23% of the annual changes in ΔO_2 and ΔCO_2, respectively (Table 1) within a period of one month (from April to May). The entire bloom period ('P_1' months: Table 1) accounts for an overall ΔO_2 increase and ΔCO_2 decrease of 59% and 56%, respectively, of the annual changes. Frajka-Williams and Rhines (2010) observed that these blooms arrive at the end of the winter convection. A mesoscale variability study by Klein and Lapeyre (2009) suggested that eddy-influenced vertical advection of nutrient rich deep waters to the surface can be the reason for such intense spring blooms. Våge et al. (2009) further presume positive correlations between the maximum winter MLD and the bloom intensity of the Labrador Sea.

The second annual surface O_2 deviation event in the Labrador Sea occurs when O_2 is gradually pushed away from its saturation towards undersaturation, starting from September/October (Fig. 5c), while $\Delta CO_2 < 0$ in the summer slowly changes towards $\Delta CO_2 \sim 0$ by winter, eventually maintaining a surface CO_2 saturation from January until the onset of the next bloom (Fig. 5c). According to the CORS results, the progressively increasing surface O_2 undersaturation in the Labrador Sea during periods P_3 and P_4 accounts for ~44% of the annual ΔO_{2chg}. The net movement of the average monthly CORS signals in a northwest direction on the CORS plot (Fig. 5c) identifies deep water convection to be the primary driver. Supporting this, a comparison between Fig. 5b and Fig. 6c show that the deep water ΔO_2 and ΔCO_2 distribution in the Labrador Sea is similar in magnitude to the surface water ΔO_2 and ΔCO_2 distribution of the P_4 period, thus confirming that the surface waters of the Labrador Sea during winter carry similar O_2-CO_2 properties as deep water at the convection depths. This is also supported by the fact that the difference between the observed and the expected y-axis intercepts (representing ΔCO_2 at constant ΔO_2) in the surface Labrador Sea (−2.8 μmol kg^{-1}; Fig. 6b) is similar to the difference between the observed and the expected ΔCO_2 (at constant ΔO_2) in the deeper Labrador Sea (−3.2 μmol kg^{-1}; Fig. 6c). The afore-mentioned '$\Delta O_2 < 0$' state persists for a period exceeding six months which strongly disagrees with our general understanding of oxygen's expected behaviour following a perturbation (Fig. 1a).

This question has been addressed by many studies (discussed later in detail), which concluded that, during winter convection, strong deepening of the MLD followed by rapid mixing of O_2-poor deep waters into the surface waters prevents sufficient O_2 transfer to the mixed layer from the atmosphere, thus maintaining the visibly persistent O_2 undersaturation in the surface Labrador Sea. The rest of this paper discusses the results from the LSM which examines this scenario with an emphasis on the individual and combined roles of the major processes that alter surface O_2 in the region.

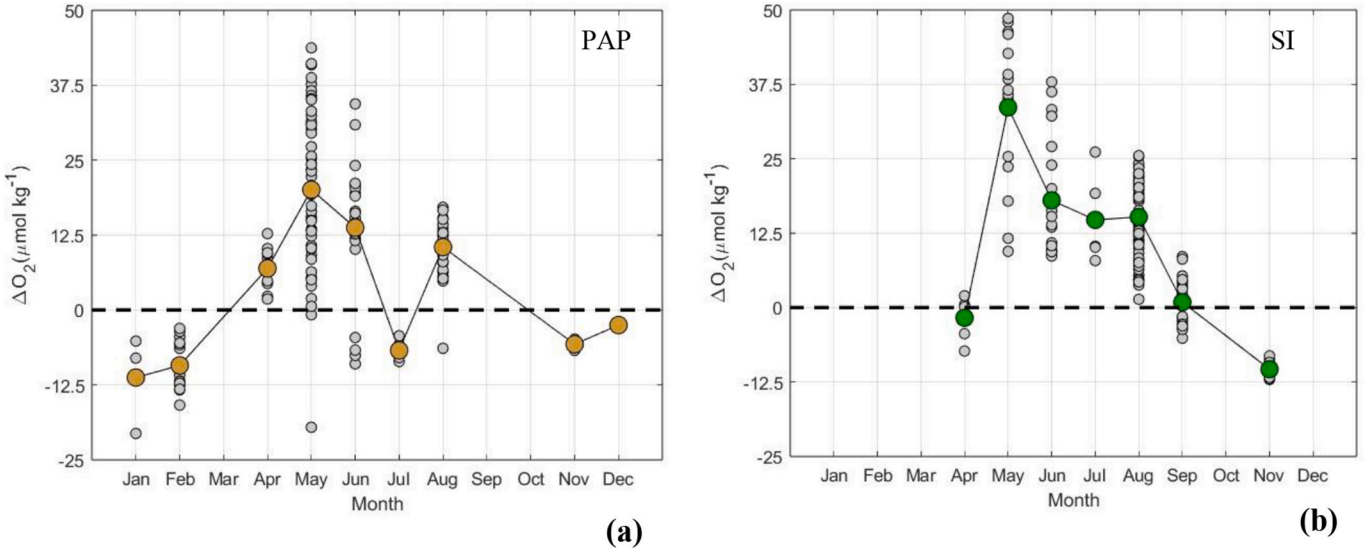

Fig. 10. Annual surface ΔO_2 cycles at the (a) PAP and (b) SI, as shown by GLODAPv2 data. Yellow (a) and green (b) circles indicate monthly averaged ΔO_2 with each month's value being the average of all data collected in that month (grey circles), regardless of which year it was collected in. (a) presents PAP data from 1981 to 2017 for the geographical region of 45°N – 53 N and 6°W – 20°W. (b) presents SI data from 1981 to 2015 for the geographical region of 55°N – 62°N and 10°W – 25°W. (For interpretation of the references to colour in this figure legend, the reader is referred to the web version of this article.)

4.2. Insights from the Labrador Sea model

Several models in the existing literature have provided insights into the Labrador Sea's persistent O_2 anomaly. Clarke and Coote (1988) presented a simple mixed layer model combined with gas exchange, in order to examine the evolution of oxygen saturation in the mixed layer. Their model used fixed values for O_2 piston velocity and was run for a maximum period of hundred days. The model elaborated the importance of the depth of the mixed layer against counteracting O_2 fluxes. A seasonal winter convection model developed by Hamme and Severinghaus (2007) used inert gases to explain response differences of thermal- and bubble-sensitive gases to disequilibriation in the Labrador Sea under deepening MLD conditions. Ito et al. (2004) modified an existing ocean circulation model (MITgcm: Massachusetts Institute of Technology General Circulation Model) by including biogeochemical processes, and examined how wintertime O_2 disequilibrium in the Labrador Sea affects Apparent Oxygen Utilization of the interior waters. Sun et al. (2017) forced the same MITgcm model with air-sea O_2 transfer via both diffusion and bubble injection to find that duration and strength of surface cooling during winter determines the degree of mixing and the intensity of the O_2 sink in the Labrador Sea.

The model presented in our study (LSM) for the first time combines major ecosystem processes in the area with biogeochemical cycling of oxygen, carbon and nitrogen. Contributions from six main drivers are considered in the model simulations: (1) photosynthesis, (2) respiration, (3) wind-dependent air-sea gas exchange, (4) vertical mixing, (5) entrainment/detrainment and (6) bubble-mediated O_2 transfer. Fig. 7 and Supplementary Fig. 2 assess the LSM's ability to reproduce the observed O_2-CO_2 trends of the Labrador Sea, and Figs. 8 and 9 show the dependence on how these factors were included. A series of experiments which estimated the magnitudes of these controls on O_2 (by switching on/off the processes listed above) suggest that spring blooms account for a maximum O_2 supersaturation of 7.2% in the region with a counteracting maximum O_2 out-flux of 0.35 mol m^{-2} day^{-1}. In the absence of this air-sea gas exchange flux, Labrador Sea blooms would push summertime O_2 towards ~30% supersaturation (Fig. 8b). The model also confirms the significance of deep winter mixing in the area on entrainment of bottom waters that acts against winter O_2 fluxes (max: 0.33 mol m^{-2} day^{-1} into the ocean). The entrainment of bottom waters pushes surface O_2 to a maximum undersaturation of 9.4%. If the model is adapted so that entrainment and convection do not follow as a consequence of mixed layer deepening then the wintertime O_2 deviation drops down to a maximum undersaturation of only 1.5%. A comparison between these model-predicted estimations for O_2 and the findings from Körtzinger et al. (2008) is given in Supplementary Table 1.

4.3. Role of different factors in producing the long-lasting O_2 undersaturation

Several previous studies elaborated the crucial role Labrador Sea's deepening winter mixed layer plays on the intensity of the region's surface O_2 anomaly: Wolf et al. (2018) used float-derived data to argue that the deeper the Labrador Sea's MLD reaches, the greater its surface O_2 undersaturation will be. Koelling et al. (2017) investigated the region's O_2 uptake during the 2014–2015 period when the wintertime MLD reached 1700 m. The estimated results were then compared to a similar study done by Körtzinger et al. (2004) for the period of 2003–2004, when the region's MLD reached to 1400 m, drawing the conclusion that winters with deeper wintertime MLDs lead to uptake of more O_2 from the atmosphere compared to the winters with relatively shallower MLDs. In agreement with these studies, this paper also confirms that the variability of the Labrador Sea's MLD is crucial in determining the magnitude of its wintertime O_2 budget: we found that the model results could only be fitted to the K1's winter data for 2004–2005 year once 'H_M' was forced with local in-situ MLD observations (MLD_{LS}) for the same time period (obtained from Körtzinger et al., 2008).

To better understand the role of the winter MLD in producing O_2 undersaturation, we left the calculations for mixing and entrainment unchanged while forcing the model with different MLD patterns (Fig. 9a). The four MLD ranges used in the LSM were chosen based on the hypothesis that shallower mixed layers would reduce the intensity of winter convection and entrainment and, therefore, would not drive a long-term O_2 undersaturation. MLD_{SI} and MLD_{PAP} are examples of mixed layer dynamics in the northern and eastern parts of the North Atlantic basin where no deep water formation occurs. These two oceanographic regions are characterised by winter mixed layers with maximum depths of ~650 m and ~400 m, respectively. However, when the 'H_M' is forced by these shallower MLDs (shallower than the MLD_{LS}), our model still fails to restore the winter O_2 anomaly, suggesting that the effect of introduction of low O_2 deep water is not outcompeted by gas exchange even at these shallower MLDs. This is, however, not the case when the winter MLD shoals to extremely low depths (max. 50 m; $MLD_{shallow}$) or is fixed at its lowest summertime value (10 m for MLD_{LS}) throughout the year (MLD_{fixed}). As expected, this last modification greatly amplifies the atmosphere's ability to dampen surface O_2 deviations in winter (H_M = 10 m should lead to 100-fold more rapid restoration of equilibrium than H_M = 1000 m). Hence, forcing the model with $MLD_{shallow}$ brings O_2 undersaturation to negligible levels (~1.5%) whereas MLD_{fixed} prevents undersaturation altogether.

These model runs confirm that the MLD deepening needs to be continuous and long-term to drive a persistent O_2 disequilibrium in the region. At the same time, the model runs imply that although the extremely deep maximum winter mixing depth in the Labrador Sea is important in determining the magnitude of the region's O_2 undersaturation (O_2 values of the model could be matched with those of the K1 data only when the H_M of the LSM was forced by MLD_{LS}), such extreme depths are not necessarily required for its long-term continuation. Even if the maximum mixing depth is only one-third of that (400 m), the effect is still severe enough to resist the air-sea gas exchange rates of O_2 and therefore to drive a prolonged anomaly (Fig. 9a). These conclusions lead to the suggestion that both PAP and SI should experience surface O_2 undersaturation in winter. In support of this, a preliminary investigation using GLODAPv2 data from near to the PAP site indicates a persistent surface O_2 undersaturation during winter (Fig. 10a), previously identified also in Porcupine Abyssal Plain Sustained Observatory (PAP-SO) data (Binetti et al., 2020; Hartman et al., 2021) but not investigated more widely. Furthermore, although GLODAPv2 data did not contain O_2 measurements for the full winter season in the SI (Fig. 10b), undersaturated O_2 values observed for November and April in the region hint at the occurrence of a similar surface O_2 undersaturation event there that persists for many months.

Sun et al. (2017) state that, during intense entrainment, surface O_2 deviations are dominated by deep O_2 deviations. Confirming this, model experiments performed by forcing the bottom layer of the LSM with O_2 concentrations higher than the observed deep water O_2 concentration for the region show the influence of bottom O_2 (Figs. 9b, c and d). The degree of wintertime O_2 undersaturation is seen to be directly linked to the bottom water [O_2]. Thus, we argue that if the bottom water is not strongly undersaturated with respect to O_2 then prolonged O_2 undersaturation will not occur in winter. Fig. 8c provides further evidence to confirm this by showing that in the absence of entrainment and therefore the influence from bottom waters, Labrador Sea's surface O_2 stays at near-equilibrium with the atmosphere.

4.4. New insights into CORS plot y-intercepts

Although the primary focus of this paper is to better understand the surface O_2 anomaly of the Labrador Sea, the results also have a wider implication. A Southern Ocean study by Wu et al. (2022) found negative y-intercepts on CORS plots for selected surface float data from the SOCCOM (Southern Ocean Carbon and Climate Observations and Modelling) project. The authors attributed these offsets to possible issues

with float data quality, stating that *"the anomalous float y-intercepts suggest offsets most likely due to pH-related biases"* in the CO_2 sensors. The y-intercepts on a CORS plot reveal the magnitude of ΔCO_2 (y-axis) when $\Delta O_2 = 0$ (x-axis). High quality GLODAPv2 data reveal that the global ocean shows near-zero y-intercepts for both quiescent and less quiescent oceanographic regions (Wu et al., 2022). Nevertheless, the CORS plots for the surface layer of the Labrador Sea (Figs. 5b and c and Fig. 6) intersect the y-axis at significantly negative ΔCO_2 values, indicating that when surface O_2 of the Labrador Sea is in equilibrium with the atmosphere ($x = 0$), surface CO_2 shows an undersaturation ($y < 0$). Our deep water CORS results for the Labrador Sea also confirm this observation by showing that the observed deep water ΔCO_2 signal is significantly lower than the expected deep water signal for respiratory CO_2, making the Labrador Sea an important sink for the gas (Martz et al., 2009; McKinley et al., 2004; Terenzi et al., 2007). Time series observations from SURATLANT data, which comprises ship-collected measurements since 1993 along transects between Iceland and Newfoundland (Reverdin et al., 2018), further suggest that this surface CO_2 anomaly can also be present across the Central North Atlantic Subtropical Gyre (Supplementary Fig. 4). Therefore the CORS results from this paper demonstrate that the negative anomalies in CORS plots' y-intercepts noted by Wu et al. (2022) can in fact be genuine and do not necessarily indicate data error. Autonomously-collected (e.g. biogeochemical float) data should not, therefore, be discarded or corrected just because it has a negative y-intercept.

5. Conclusions

This paper improves understanding of the Labrador Sea's persistent surface O_2 undersaturation by analysing results from two novel approaches: (1) observations plotted using the CORS method, and (2) simulations using a coupled ecosystem-biogeochemical model. The model introduced here examines the biological and physical forcing in the region and successfully reproduces the observed magnitudes of the O_2 anomalies and fluxes. The study also elucidates the combined influence of the deepening mixed layer, winter convection, deep water entrainment and bottom water O_2 concentrations in maintaining a persistent surface O_2 undersaturation in winter despite the counteracting effects of air-sea gas exchange. Our model experiments indicate that the long-lasting nature of the region's O_2 undersaturation is not exclusively caused by the great depth of mixing in winter. Rather, it is suggested that even maximum mixing depths only a third as deep (400 m instead of 1200 m) will produce similar O_2 behaviour at the surface, as long as the deep water is also O_2-depleted and is continuously entrained to the surface. This hypothesis could be tested in future O_2 investigations in the North Atlantic basin. Moreover, this study also shows that non-zero y-axis intercepts on CORS plots can be genuine and therefore should not automatically be assumed to indicate data error.

Code availability

The computational codes are available upon request to A.S.

Author contribution

A.S. and T.T. conceived the presented idea and designed the study. A. S. performed computational framework, designed the model, carried out simulations and wrote the manuscript in consultation with T.T. In addition, T.T., D.P. and N.B. supervised the findings of this study. All authors provided critical feedback and helped shape the study, analysis and article.

Funding

This work was supported by the Presidential Scholarship Scheme 2020 of the University of Southampton, United Kingdom.

CRediT authorship contribution statement

Amavi N. Silva: Writing – original draft, Visualization, Validation, Methodology, Investigation, Formal analysis, Data curation, Conceptualization. **Duncan A. Purdie:** Writing – review & editing, Visualization, Validation, Supervision. **Nicholas R. Bates:** Writing – review & editing, Visualization, Validation, Supervision. **Toby Tyrrell:** Writing – review & editing, Supervision, Methodology, Investigation, Conceptualization.

Declaration of Competing Interest

The authors declare that they have no known competing financial interests or personal relationships that could have appeared to influence the work reported in this paper.

Data availability

Quality controlled bottle data from the Global Ocean Data Analysis Project version 2_2023 (GLODAPv2.2023) data product was downloaded from https://glodap.info/index.php/merged-and-adjusted-data-product-v2-2023/. The K1 and SURATLANT data were provided upon request from GEOMAR: Helmholtz-Centre for Ocean Research Kiel and the French National Centre for Scientific Research, respectively. Local in-situ sea level pressure, daily wind speed, monthly mixed layer depth values were obtained from reanalysis products from National Center for Environmental Prediction/National Center for Atmospheric Research (NCEP/NCAR) (https://psl.noaa.gov/data/gridded/data.ncep.reanalysis.surface.html). Atmospheric CO_2 mole fraction in dry air was obtained from the globally averaged surface annual mean data published in https://www.esrl.noaa.gov/gmd/ccgg/trends/.

Acknowledgements

We would like to thank Dr. Arne Körtzinger of GEOMAR: Helmholtz-Centre for Ocean Research, Kiel and Dr. Nicolas Metzl of French National Centre for Scientific Research for their support in providing requested datasets. We also acknowledge the data generators and synthesizers of the GLODAP data product.

Appendix A. Appendix

Except where otherwise mentioned, the values of the model parameters in this section are for 60°N in the North Atlantic Ocean (as presented in Taylor et al., 1991 and Tyrrell and Taylor, 1995). In the model eqs. 5 to 14, 'α' represents the phytoplankton growth rate as a product of irradiance (I) and temperature (T) while 'φ' is the nutrient (N) dependent growth rate where both I and N behave according to Michaelis-Menten kinetics. Peak daily irradiance (I_{max}) (used to calculate light intensities of the mixed layer (I_M) and the thermocline (I_T)) was computed according to Kirk (1994). Surface irradiance (I_{surf}) for the thermocline was assumed to be equal to the light intensity at the mixed layer-thermocline interface. When surface irradiance is zero for a given time of the day, the corresponding I_{surf} was taken as zero. 'E_{go}', the background extinction coefficient of green light when chlorophyll is absent, was used to calculate extinction coefficients of red (E_r) and green (E_g) lights when chlorophyll is present. 'γ' describes the nutrient content of the phytoplankton cell which is the carbon to chlorophyll ratio divided by 14.01 times of carbon to nitrogen ratio. The parameter 'm' stands for the loss rate due to phytoplankton mortality, zooplankton grazing and remineralization. 'ε', the recycling efficiency, describes the nutrient fraction that is

being returned to solution upon cell loss, and has the same value as 'ε_C', the fraction of carbon present in phytoplankton which is returned back to solution upon cell loss (i.e. mortality, grazing, respiration). 'v' is the sinking velocity of particulate organic matter.

In the LSM, turbulent diffusion rates between the layers were assumed to be proportional to their concentration differences. 'k_1' describes mixing between the thermocline and the bottom layer while 'k_2' describes that between the mixed layer and the thermocline. They were both considered to be functions of H_M only. Maximum temperature (T_{max}), minimum temperature (T_{min}) and P_B values for the Labrador Sea were taken from Körtzinger et al. (2008). T_M and salinity (sal) were forced by the monthly variations in SST and SSS in the K1 site, respectively. N_B was forced by the average deep nitrate concentration in the Labrador Sea (6.0 μmol kg^{-1}), calculated from the GLODAPv2 data.

'τ_A' stands for the conversion factor of mmol m^{-3} to μmol kg^{-1}. 'τ_C' explains the reduction (increase) of carbon (oxygen) in the water when 1.0 mg m^{-3} of organic matter is produced while 'τ_C*' describes the increase (reduction) of carbon (oxygen) when 1.0 mg m^{-3} of organic matter is remineralized. Both these parameters are equal to the carbon to chlorophyll ratio divided by $12 \times 10^6 \times 1.025$.

'p_{air}' and 'p_m' stand for pCO_2 in the atmosphere and the mixed layer, respectively. p_{air} was forced by average annual partial pressure of CO_2 observed for the Labrador Sea (Körtzinger et al., 2008) whereas p_m was calculated using CSYS software (Zeebe and Wolf-Gladrow, 2001) from TA and DIC. 'K_{CO2}' describes the transfer rate of CO_2 across the sea surface which is equal to the piston velocity multiplied by the CO_2 solubility in sea water (calculated from Weiss, 1974).

Piston velocities for O_2 (G_O) and CO_2 (G_C) were calculated as a function of surface wind speed (Supplementary Fig. 5), using the cubically approximated equation proposed by Wanninkhof (1992) and modified by Kihm and Körtzinger (2010) to better represent the Labrador Sea:

$$G = 0.029 \times u^3 \times (Sc/660)^{-0.5} \quad \text{(A1)}$$

'G' expresses either G_O or G_C (cm hr^{-1}). 'u' stands for wind speed (m s^{-1}). '*Sc*' is the Schmidt number for either O_2 or CO_2 at the mixed layer temperature (T_M) whereas 660 is a normalized value for S_C. S_C for the two gases was calculated using coefficients given in Wanninkhof (1992):

$$S_C \text{ for } O_2 = 1953.4 - 128 \times T_M + 3.9918 \times T_M^2 - 0.050091 \times T_M^3 \quad \text{(A2)}$$

$$S_C \text{ for } CO_2 = 2073.1 - 125.62 \times T_M + 3.6276 \times T_M^2 - 0.043219 \times T_M^3 \quad \text{(A2)}$$

'q' gives the photosynthetic quotient which is considered to be 1.5 when the growth of a blooming event is ongoing with nitrate mainly being utilized. 'O_{sat}' is the saturated concentration of O_2 in the surface which was computed based on the O_2 solubility equation proposed by Garcia and Gordon (1992, 1993).

Table A.1
Parameters and their values used in the LSM (Sources: Kirk, 1994; Körtzinger et al., 2008; Taylor et al., 1991; Tyrrell and Taylor, 1995; GLODAPv2 data).

Parameter	Symbol	Unit	Value
Thermocline layer of thickness	H_T	m	40.0
Nutrient recyling efficiency	ε		0.2
Particle sinking velocity	v	m d^{-1}	0.9
Nutrient half saturation constant	N_h	mmol N m^{-3}	0.1
Light half saturation constant	I_h	W m^{-2}	10.0
Solar constant	SC	W m^{-2}	1373
Maximum growth rate	α_{max}	d^{-1}	2.0
Maximum temperature	T_{max}	°C	8.0
Minimum temperature	T_{min}	°C	3.0
Bottom temperature	T_B	°C	1.0
Carbon: Chlrophyl ratio			40.0
Carbon: Nitrogen ratio			5.6
Bottom phytoplankton abundance	P_B	mg Chl-a m^{-3}	0.25
Bottom nutrient concentration	N_B	mmol N m^{-3}	10.0
Background extinction coefficient for green light (when cholorophyll is absent)	E_{go}	m^{-1}	0.08
Maximum mortality	m_{max}	d^{-1}	0.1
Minimum mortality	m_{min}	d^{-1}	0.02
Diffusion coefficient between thermocline and bottom layer	k_{1s}	m d^{-1}	0.6
Diffusion coefficient between mixed layer and thermocline	k_{2s}	m d^{-1}	0.6
Latitude	g	°N	56
Conversion factor of mmol N m^{-3} to mol kg^{-1}	τ_A		−1.025
Bottom alkalinity	A_B	μmol kg^{-1}	2300
Photosynethetic quotient	q		1.5
Carbon recyling efficiency	ε_c		0.2
Bottom O_2 concentration	O_B	μmol kg^{-1}	290
Bottom DIC concentration	C_B	μmol kg^{-1}	2155

Appendix B. Supplementary data

Supplementary data to this article can be found online at https://doi.org/10.1016/j.jmarsys.2024.103996.

References

Anderson, L.A., Sarmiento, J.L., 1994. Redfield ratios of remineralization determined by nutrient data analysis. Glob. Biogeochem. Cycles 8 (1), 65–80. https://doi.org/10.1029/93gb03318.

Atamanchuk, D., Koelling, J., Send, U., Wallace, D.W.R., 2020. Rapid transfer of oxygen to the deep ocean mediated by bubbles. Nat. Geosci. 13 (3), 232–237. https://doi.org/10.1038/s41561-020-0532-2.

Avsic, T., Karstensen, J., Send, U., Fischer, J., 2006. Interannual variability of newly formed Labrador Sea water from 1994 to 2005. Geophys. Res. Lett. 33 (21) https://doi.org/10.1029/2006gl026913.

Bacon, S., Gould, W.J., Jia, Y., 2003. Open-ocean convection in the Irminger Sea. Geophys. Res. Lett. 30 (5) https://doi.org/10.1029/2002gl016271 p.n/a-n/a.

Binetti, U., Kaiser, J., Damerell, G.M., Rumyantseva, A., Martin, A.P., Henson, S., Heywood, K.J., 2020. Net community oxygen production derived from Seaglider deployments at the porcupine abyssal plain site (PAP; Northeast Atlantic) in 2012–13. Prog. Oceanogr. 183, 102293 https://doi.org/10.1016/j.pocean.2020.102293.

Blomquist, B.W., Brumer, S.E., Fairall, C.W., Huebert, B.J., Zappa, C.J., Brooks, I.M., Yang, M., Bariteau, L., Prytherch, J., Hare, J.E., Czerski, H., Matei, A., Pascal, R.W., 2017. Wind speed and sea state dependencies of Air-Sea gas transfer: results from the high wind speed gas exchange study (HiWinGS). J. Geophys. Res. Oceans 122 (10), 8034–8062. https://doi.org/10.1002/2017jc013181.

Bograd, S.J., Castro, C.G., Di Lorenzo, E., Palacios, D.M., Bailey, H., Gilly, W., Chavez, F. P., 2008. Oxygen declines and the shoaling of the hypoxic boundary in the California Current. Geophys. Res. Lett. 35 (12) https://doi.org/10.1029/2008gl034185 n/a-n/a.

Boyer, T.P., Antonov, J.I., Baranova, O.K., Coleman, C., Garcia, H.E., Grodsky, A., Johnson, D.R., Locarnini, R.A., Mishonov, A.V., O'Brien, T.D., Paver, C.R., Reagan, J. R., Seidov, D., Smolyar, I.V., Zweng, M.M., 2013. World ocean database 2013. In: Levitus, Sydney, Mishonov, Alexey (Eds.), NOAA Atlas NESDIS 72. https://doi.org/10.7289/V5NZ85M, 209 pp.

Broecker, W.S., Peng, T.-H., 1982. Tracers in the Sea. Palisades, Ny Lamont-Doherty Geolog. Observatory, Columbia Univ.

Bushinsky, S.M., Gray, A.R., Johnson, K.S., Sarmiento, J.L., 2017. Oxygen in the Southern Ocean from Argo floats: determination of processes driving Air-Sea fluxes. J. Geophys. Res. Oceans 122 (11), 8661–8682. https://doi.org/10.1002/2017jc012923.

Carrillo, C.J., Smith, R.C., Karl, D.M., 2004. Processes regulating oxygen and carbon dioxide in surface waters west of the Antarctic peninsula. Mar. Chem. 84 (3–4), 161–179. https://doi.org/10.1016/j.marchem.2003.07.004.

Centurioni, L.R., Gould, W.J., 2004. Winter conditions in the Irminger Sea observed with profiling floats. J. Mar. Res. 62 (3), 313–336. https://doi.org/10.1357/0022240041446209.

Clarke, R.A., Coote, A.R., 1988. The formation of Labrador Sea water. Part III: the evolution of oxygen and nutrient concentration. J. Phys. Oceanogr. 18 (3), 469–480. https://doi.org/10.1175/1520-0485(1988)018%3C0469:tfolsw%3E2.0.co;2.

Conkright, M.E., Locarnini, R.A., Garcia, H.E., O'Brien, T.D., Boyer, T.P., Stephens, C., Antonov, J.I., 2002. World Ocean Atlas 2001: Objective Analyses, Data Statistics, and Figures, CD-ROM Documentation. National Oceanographic Data Center, Silver Spring, MD, p. 17.

Craig, H., Hayward, T., 1987. Oxygen supersaturation in the ocean: biological versus physical contributions. Science 235 (4785), 199–202. https://doi.org/10.1126/science.235.4785.199.

Curry, R.G., McCartney, M.S., Joyce, T.M., 1998. Oceanic transport of subpolar climate signals to mid-depth subtropical waters. Nature 391 (6667), 575–577. https://doi.org/10.1038/35356.

de Jong, M.F., van Aken, H.M., Våge, K., Pickart, R.S., 2012. Convective mixing in the central Irminger Sea: 2002–2010. Deep-Sea Res. I Oceanogr. Res. Pap. 63, 36–51. https://doi.org/10.1016/j.dsr.2012.01.003.

DeGrandpre, M.D., Hammar, T.R., Smith, S.P., Sayles, F.L., 1995. In situ measurements of seawater pCO_2. Limnol. Oceanogr. 40 (5), 969–975. https://doi.org/10.4319/lo.1995.40.5.0969.

Dickson, A.G., 1990. Standard potential of the reaction: $AgCl(s) + 12H_2(g) = ag(s) + HCl(aq)$ and the standard acidity constant of the ion HSO_4^- in synthetic sea water from 273.15 to 318.15 K. J. Chem. Thermodyn. 22 (2), 113–127. https://doi.org/10.1016/0021-9614(90)90074-z.

Duteil, O., Koeve, W., Oschlies, A., Bianchi, D., Galbraith, E., Kriest, I., Matear, R., 2013. A novel estimate of ocean oxygen utilisation points to a reduced rate of respiration in the ocean interior. Biogeosciences 10 (11), 7723–7738. https://doi.org/10.5194/bg-10-7723-2013.

Emerson, S., 1987. Seasonal oxygen cycles and biological new production in surface waters of the subarctic Pacific Ocean. J. Geophys. Res. 92 (C6), 6535. https://doi.org/10.1029/jc092ic06p06535.

Emerson, S., Stump, C., 2010. Net biological oxygen production in the ocean—II: remote in situ measurements of O_2 and N_2 in subarctic pacific surface waters. Deep-Sea Res. I Oceanogr. Res. Pap. 57 (10), 1255–1265. https://doi.org/10.1016/j.dsr.2010.06.001.

Frajka-Williams, E., Rhines, P.B., 2010. Physical controls and interannual variability of the Labrador Sea spring phytoplankton bloom in distinct regions. Deep-Sea Res. I Oceanogr. Res. Pap. 57 (4), 541–552. https://doi.org/10.1016/j.dsr.2010.01.003.

Frajka-Williams, E., Rhines, P.B., Eriksen, C.W., 2009. Physical controls and mesoscale variability in the Labrador Sea spring phytoplankton bloom observed by Seaglider. Deep-Sea Res. I Oceanogr. Res. Pap. 56 (12), 2144–2161. https://doi.org/10.1016/j.dsr.2009.07.008.

Garcia, H.E., Gordon, L.I., 1992. Oxygen solubility in seawater: better fitting equations. Limnol. Oceanogr. 37 (6), 1307–1312. https://doi.org/10.4319/lo.1992.37.6.1307.

Garcia, H.E., Gordon, L.I., 1993. Erratum: oxygen solubility in seawater: better fitting equations. Limnolog. Ocenogr. 38 (3).

Garcia, H.E., Boyer, T.P., Baranova, O.K., Locarnini, R.A., Mishonov, A.V., Grodsky, A., Paver, C.R., Weathers, K.W., Smolyar, I.V., Reagan, J.R., Seidov, D., Zweng, M.M., 2019. World Ocean Atlas 2018: Product Documentation.

Giomi, F., Barausse, A., Duarte, C.M., Booth, J., Agusti, S., Saderne, V., Anton, A., Daffonchio, D., Fusi, M., 2019. Oxygen supersaturation protects coastal marine fauna from ocean warming. Sci. Adv. 5 (9), eaax1814. https://doi.org/10.1126/sciadv.aax1814.

Gordon, A.L., Huber, B.A., 1990. Southern Ocean winter mixed layer. J. Geophys. Res. 95 (C7), 11655. https://doi.org/10.1029/jc095ic07p11655.

Hamme, R.C., Severinghaus, J.P., 2007. Trace gas disequilibria during deep-water formation. Deep-Sea Res. I Oceanogr. Res. Pap. 54 (6), 939–950. https://doi.org/10.1016/j.dsr.2007.03.008.

Hamme, R.C., Emerson, S., Severinghaus, J.P., Long, M.C., Yashayaev, I., 2017. Using Noble gas measurements to derive Air-Sea process information and predict physical gas saturations. Geophys. Res. Lett. 44 (19), 9901–9909. https://doi.org/10.1002/2017gl075123.

Hartman, S.E., Bett, B.J., Durden, J.M., Henson, S.A., Iversen, M., Jeffreys, R.M., Horton, T., Lampitt, R., Gates, A.R., 2021. Enduring science: three decades of observing the Northeast Atlantic from the porcupine abyssal plain sustained observatory (PAP-SO). Prog. Oceanogr. 191, 102508 https://doi.org/10.1016/j.pocean.2020.102508.

Head, E., Harris, L.R., Campbell, R.W., 2000. Investigations on the ecology of *Calanus spp.* in the Labrador Sea. I. Relationship between the phytoplankton bloom and reproduction and development of *Calanus finmarchicus* in spring. Mar. Ecol. Prog. Ser. 193, 53–73. https://doi.org/10.3354/meps193053.

Ito, T., Follows, M.J., Boyle, E.A., 2004. Is AOU a good measure of respiration in the oceans? Geophys. Res. Lett. 31 (17) https://doi.org/10.1029/2004gl020900 p.n/a-n/a.

Ito, T., Hamme, R.C., Emerson, S., 2011. Temporal and spatial variability of noble gas tracers in the North Pacific. J. Geophys. Res. 116 (C8) https://doi.org/10.1029/2010jc006828.

Kara, A.B., Rochford, P.A., Hurlburt, H.E., 2003. Mixed layer depth variability over the global ocean. J. Geophys. Res. 108 (C3) https://doi.org/10.1029/2000jc000736.

Keeling, R.F., 1993. On the role of large bubbles in air-sea gas exchange and supersaturation in the ocean. J. Mar. Res. 51 (2), 237–271. https://doi.org/10.1357/0022240933223800.

Keeling, R.F., Stephens, B.B., Najjar, R.G., Doney, S.C., Archer, D., Heimann, M., 1998. Seasonal variations in the atmospheric O_2/N_2 ratio in relation to the kinetics of air-sea gas exchange. Glob. Biogeochem. Cycles 12 (1), 141–163. https://doi.org/10.1029/97gb02339.

Kieke, D., Yashayaev, I., 2015. Studies of Labrador Sea water formation and variability in the subpolar North Atlantic in the light of international partnership and collaboration. Progress Oceanogr. 132, 220–232. https://doi.org/10.1016/j.pocean.2014.12.010.

Kihm, C., Körtzinger, A., 2010. Air-sea gas transfer velocity for oxygen derived from float data. J. Geophys. Res. 115 (C12) https://doi.org/10.1029/2009jc006077.

Kirk, J.T.O., 1994. Light and Photosynthesis in Aquatic Ecosystems. Cambridge University Press.

Kistler, R., Collins, W., Saha, S., White, G., Woollen, J., Kalnay, E., Chelliah, M., Ebisuzaki, W., Kanamitsu, M., Kousky, V., van den Dool, H., Jenne, R., Fiorino, M., 2001. The NCEP–NCAR 50–year reanalysis: monthly means CD–ROM and documentation. Bull. Am. Meteorol. Soc. 82 (2), 247–267. https://doi.org/10.1175/1520-0477(2001)082%3C0247:tnnyrm%3E2.3.co;2.

Klein, P., Lapeyre, G., 2009. The oceanic vertical pump induced by mesoscale and submesoscale turbulence. Annu. Rev. Mar. Sci. 1 (1), 351–375. https://doi.org/10.1146/annurev.marine.010908.163704.

Koelling, J., Wallace, D.W.R., Send, U., Karstensen, J., 2017. Intense oceanic uptake of oxygen during 2014-2015 winter convection in the Labrador Sea. Geophys. Res. Lett. 44 (15), 7855–7864. https://doi.org/10.1002/2017gl073933.

Koelling, J., Atamanchuk, D., Karstensen, J., Handmann, P., Wallace, D.W.R., 2022. Oxygen export to the deep ocean following Labrador Sea water formation. Biogeosciences 19 (2), 437–454. https://doi.org/10.5194/bg-19-437-2022.

Körtzinger, A., Schimanski, J., Send, U., Wallace, D., 2004. The ocean takes a deep breath. Science 306 (5700), 1337. https://doi.org/10.1126/science.1102557.

Körtzinger, A., Schimanski, J., Send, U., 2005. High quality oxygen measurements from profiling floats: A promising new technique. J. Atmos. Ocean. Technol. 22 (3), 302–308. https://doi.org/10.1175/jtech1701.1.

Körtzinger, A., Send, U., Wallace, D.W.R., Karstensen, J., DeGrandpre, M., 2008. Seasonal cycle of O_2 and pCO_2 in the Central Labrador Sea: atmospheric, biological, and physical implications. Glob. Biogeochem. Cycles 22 (1). https://doi.org/10.1029/2007gb003029 p.n/a-n/a.

Lauvset, S.K., Lange, N., Tanhua, Toste, Bittig, H.C., Olsen, A., Kozyr, A., Alin, S.R., Álvarez, M., Azetsu-Scott, Kumiko, Barbero, L., Becker, S., Brown, P.J., Carter, B.R., Feely, R.A., Hoppema, M., Humphreys, M., Ishii, M., Jeansson, E., Jiang, L., 2022. GLODAPv2.2022: the latest version of the global interior ocean biogeochemical data product. Earth System Sci.Data 14 (12), 5543–5572. https://doi.org/10.5194/essd-14-5543-2022.

Lavender, K.L., Davis, R.E., Owens, W.B., 2002. Observations of Open-Ocean deep convection in the Labrador Sea from subsurface floats. J. Phys. Oceanogr. 32 (2), 511–526. https://doi.org/10.1175/1520-0485(2002)032%3C0511:oooodc%3E2.0.co;2.

Lazier, J.R.N., 1973. The renewal of Labrador Sea water. Deep-Sea Res. Oceanogr. Abstr. 20 (4), 341–353. https://doi.org/10.1016/0011-7471(73)90058-2.
Longhurst, A., 2007. Ecological Geography of the Sea. Academic Press, Burlington, Ma, Usa.
Lueker, T.J., Dickson, A.G., Keeling, C.D., 2000. Ocean pCO_2 calculated from dissolved inorganic carbon, alkalinity, and equations for K_1 and K_2: validation based on laboratory measurements of CO_2 in gas and seawater at equilibrium. Mar. Chem. 70 (1–3), 105–119. https://doi.org/10.1016/s0304-4203(00)00022-0.
Manabe, S., Stouffer, R.J., 1993. Century-scale effects of increased atmospheric CO_2 on the ocean–atmosphere system. Nature 364 (6434), 215–218. https://doi.org/10.1038/364215a0.
Marshall, J., Schott, F., 1999. Open-ocean convection: observations, theory, and models. Rev. Geophys. 37 (1), 1–64. https://doi.org/10.1029/98rg02739.
Martz, T.R., DeGrandpre, M.D., Strutton, P.G., McGillis, W.R., Drennan, W.M., 2009. Sea surface pCO_2 and carbon export during the Labrador Sea spring-summer bloom: an in situ mass balance approach. J. Geophys. Res. 114 (C9) https://doi.org/10.1029/2008jc005060.
Matear, R.J., Hirst, A.C., McNeil, B.I., 2000. Changes in dissolved oxygen in the Southern Ocean with climate change. Geochem. Geophys. Geosyst. 1 (11) https://doi.org/10.1029/2000gc000086 p.n/a-n/a.
McKinley, G.A., Follows, M.J., Marshall, J., Fan, S., 2003. Interannual variability of air-sea O_2 fluxes and the determination of CO_2 sinks using atmospheric O_2/N_2. Geophys. Res. Lett. 30 (3) https://doi.org/10.1029/2002gl016044.
McKinley, G.A., Follows, M.J., Marshall, J., 2004. Mechanisms of air-sea CO_2 flux variability in the equatorial Pacific and the North Atlantic. Glob. Biogeochem. Cycles 18 (2). https://doi.org/10.1029/2003gb002179 p.n/a-n/a.
Memery, L., Merlivat, L., 1985. Modelling of gas flux through bubbles at the air-water interface. Tellus B 37B (4–5), 272–285. https://doi.org/10.1111/j.1600-0889.1985.tb00075.x.
Monahan, E.C., Torgersen, T., 1991. The enhancement of air-sea gas exchange by oceanic whitecapping. In: Water Quality Issues at Fossil Fuel Plants. ASCE, pp. 608–617.
Najjar, R.G., Keeling, R.F., 1997. Analysis of the mean annual cycle of the dissolved oxygen anomaly in the World Ocean. J. Mar. Res. 55 (1), 117–151. https://doi.org/10.1357/0022240973224481.
Olsen, A., Lange, N., Key, R., Tanhua, T., Bittig, H., Kozyr, A., Álvarez, M., Azetsu-Scott, K., Becker, S., Brown, P., Carter, B., Cotrim da Cunha, L., Feely, R.A., van Heuven, S., Hoppema, M., Ishii, M., Jeansson, E., Jutterström, S., Landa, C.S., Lauvset, S., Michaelis, P., Murata, A., Pérez, F.F., Pfeil, B., Schirnick, C., Steinfeldt, R., Suzuki, T., Tilbrook, B., Velo, A., Wanninkhof, R., Woosley, R.J., 2020. GLODAPv2.2020 – the second update of GLODAPv2. Earth System Sci. Data Discuss. https://doi.org/10.5194/essd-2020-165.
Oschlies, A., Brandt, P., Stramma, L., Schmidtko, S., 2018. Drivers and mechanisms of ocean deoxygenation. Nat. Geosci. 11 (7), 467–473. https://doi.org/10.1038/s41561-018-0152-2.
Pickart, R.S., Torres, D.J., Clarke, R.A., 2002. Hydrography of the Labrador Sea during active convection. J. Phys. Oceanogr. 32 (2), 428–457.
Reverdin, G., Metzl, N., Olafsdottir, S., Racapé, V., Takahashi, T., Benetti, M., Valdimarsson, H., Benoit-Cattin, A., Danielsen, M., Fin, J., Naamar, A., Pierrot, D., Sullivan, K., Bringas, F., Goni, G., 2018. SURATLANT: a 1993–2017 surface sampling in the central part of the North Atlantic subpolar gyre. Earth System Sci.Data 10 (4), 1901–1924. https://doi.org/10.5194/essd-10-1901-2018.
Rhein, M., Steinfeldt, R., Kieke, D., Stendardo, I., Yashayaev, I., 2017. Ventilation variability of Labrador Sea water and its impact on oxygen and anthropogenic carbon: a review. Philos. Transact. Series A, Math. Phys. Eng. Sci. 375 (2102) https://doi.org/10.1098/rsta.2016.0321.
Russell, J.L., Dickson, A.G., 2003. Variability in oxygen and nutrients in South Pacific Antarctic intermediate water. Glob. Biogeochem. Cycles 17 (2). https://doi.org/10.1029/2000gb001317 p.n/a-n/a.
Sarmiento, J.L., Gruber, N., 2006. Ocean Biogeochemical Dynamics. Princeton University Press, Princeton.
Schmidtko, S., Stramma, L., Visbeck, M., 2017. Decline in global oceanic oxygen content during the past five decades. Nature 542 (7641), 335–339. https://doi.org/10.1038/nature21399.
Schulze, L.M., Pickart, R.S., Moore, G.W.K., 2016. Atmospheric forcing during active convection in the Labrador Sea and its impact on mixed-layer depth. J. Geophys. Res. Oceans 121 (9), 6978–6992. https://doi.org/10.1002/2015jc011607.
Seltzer, A.M., Nicholson, D.P., Smethie, W.M., Tyne, R., Le Roy, Emilie, Rachel, Stute, Barry, P.H., McPaul, K., Davidson, P.W., Chang, B.X., Rafter, P.A., Lethaby, P., Johnson, R.J., Khatiwala, S., Jenkins, W.J., 2023. Dissolved gases in the deep North Atlantic track ocean ventilation processes. Proc. Natl. Acad. Sci. USA 120 (11). https://doi.org/10.1073/pnas.2217946120.
Stramma, L., Johnson, G.C., Sprintall, J., Mohrholz, V., 2008. Expanding oxygen-minimum zones in the tropical oceans. Science 320 (5876), 655–658. https://doi.org/10.1126/science.1153847.
Sun, D., Ito, T., Bracco, A., 2017. Oceanic uptake of oxygen during deep convection events through diffusive and bubble-mediated gas exchange. Glob. Biogeochem. Cycles 31 (10), 1579–1591. https://doi.org/10.1002/2017gb005716.
Takahashi, T., Sutherland, S.C., Wanninkhof, R., Sweeney, C., Feely, R.A., Chipman, D. W., Hales, B., Friederich, G., 2009. Climatological mean and decadal change in surface ocean pCO_2, and net sea–air CO_2 flux over the global oceans. *Deep Sea Research Part II: Topical Studies in Oceanography*, [online] 56 (8–10), 554–577. https://doi.org/10.1016/j.dsr2.2008.12.009.
Taylor, A.H., Watson, A.J., Ainsworth, M., Robertson, J.E., Turner, D.R., 1991. A modelling investigation of the role of phytoplankton in the balance of carbon at the surface of the North Atlantic. Glob. Biogeochem. Cycles 5 (2), 151–171. https://doi.org/10.1029/91gb00305.
Tengberg, A., Hovdenes, J., Andersson, H.J., Brocandel, O., Diaz, R., Hebert, D., Arnerich, T., Huber, C., Körtzinger, A., Khripounoff, A., Rey, F., Rönning, C., Schimanski, J., Sommer, S., Stangelmayer, A., 2006. Evaluation of a lifetime-based optode to measure oxygen in aquatic systems. Limnol. Oceanogr. Methods 4 (2), 7–17. https://doi.org/10.4319/lom.2006.4.7.
Terenzi, F., Hall, T.M., Khatiwala, S., Rodehacke, C.B., LeBel, D.A., 2007. Uptake of natural and anthropogenic carbon by the Labrador Sea. Geophys. Res. Lett. 34 (6) https://doi.org/10.1029/2006gl028543.
Tortell, P.D., Asher, E.C., Ducklow, H.W., Goldman, J.A.L., Dacey, J.W.H., Grzymski, J. J., Young, J.N., Kranz, S.A., Bernard, K.S., Morel, F.M.M., 2014. Metabolic balance of coastal Antarctic waters revealed by autonomous pCO_2 and $\Delta O_2/Ar$ measurements. Geophys. Res. Lett. 41 (19), 6803–6810. https://doi.org/10.1002/2014gl061266.
Tyrrell, T., Taylor, A.H., 1995. Latitudinal and seasonal variations in carbon dioxide and oxygen in the Northeast Atlantic and the effects on *Emiliania huxleyi* and other phytoplankton. Glob. Biogeochem. Cycles 9 (4), 585–604. https://doi.org/10.1029/95gb01133.
Vachon, D., Sadro, S., Bogard, M.J., Lapierre, J., Baulch, H.M., Rusak, J.A., Denfeld, B.A., Laas, A., Klaus, M., Karlsson, J., Weyhenmeyer, G.A., Giorgio, P.A., 2020. Paired O_2–CO_2 measurements provide emergent insights into aquatic ecosystem function. Limnol. Oceanogr. Letters 5 (4), 287–294. https://doi.org/10.1002/lol2.10135.
Våge, K., Pickart, R.S., Thierry, V., Reverdin, G., Lee, C.M., Petrie, B., Agnew, T.A., Wong, A.E., Ribergaard, M.H., 2009. Surprising return of deep convection to the subpolar North Atlantic Ocean in winter 2007–2008. Nat. Geosci. 2 https://doi.org/10.1038/ngeo382.
van Heuven, S., Pierrot, D., Rae, J.W.B., Lewis, E., Wallace, D.W.R., 2011. MATLAB Program Developed for CO_2 System Calculations; ORNL/CDIAC - 105b. Oak Ridge National Laboratory, U.S. Department of Energy, Oak Ridge, Tennessee.
Weiss, R.F., 1974. Carbon dioxide in water and seawater: the solubility of a non-ideal gas. Mar. Chem. 2 (3), 203–215. https://doi.org/10.1016/0304-4203(74)90015-2.
Weiss, R.F., Price, B.A., 1980. Nitrous oxide solubility in water and seawater. Mar. Chem. 8 (4), 347–359. https://doi.org/10.1016/0304-4203(80)90024-9.
Whitney, F.A., Freeland, H.J., Robert, M., 2007. Persistently declining oxygen levels in the interior waters of the eastern subarctic Pacific. Prog. Oceanogr. 75 (2), 179–199. https://doi.org/10.1016/j.pocean.2007.08.007.
Wolf, M.K., Hamme, R.C., Gilbert, D., Yashayaev, I., Thierry, V., 2018. Oxygen saturation surrounding deep water formation events in the Labrador Sea from Argo-O_2 data. Glob. Biogeochem. Cycles 32 (4), 635–653. https://doi.org/10.1002/2017gb005829.
Wood, R.A., Keen, A.B., Mitchell, J.F.B., Gregory, J.M., 1999. Changing spatial structure of the thermohaline circulation in response to atmospheric CO_2 forcing in a climate model. Nature 399 (6736), 572–575. https://doi.org/10.1038/21170.
Woolf, D.K., Thorpe, S.A., 1991. Bubbles and the air-sea exchange of gases in near-saturation conditions, 49 (3), 435–466. https://doi.org/10.1357/002224091784995765.
Woolf, D.K., Leifer, I.S., Nightingale, P.D., Rhee, T.S., Bowyer, P., Caulliez, G., de Leeuw, G., Larsen, S.E., Liddicoat, M., Baker, J., Andreae, M.O., 2007. Modelling of bubble-mediated gas transfer: fundamental principles and a laboratory test. J. Mar. Syst. 66 (1–4), 71–91. https://doi.org/10.1016/j.jmarsys.2006.02.011.
Wu, Y., Platt, T., Tang, C., Sathyendranath, S., 2008. Regional differences in the timing of the spring bloom in the Labrador Sea. Mar. Ecol. Prog. Ser. 355, 9–20. https://doi.org/10.3354/meps07233.
Wu, Y., Bakker, D.C.E., Achterberg, E.P., Silva, A.N., Pickup, D.D., Li, X., Hartman, S., Stappard, D., Qi, D., Tyrrell, T., 2022. Integrated analysis of carbon dioxide and oxygen concentrations as a quality control of ocean float data. Communicat. Earth & Environ. 3 (1), 1–11. https://doi.org/10.1038/s43247-022-00421-w.
Wyrtki, K., 1962. The oxygen minima in relation to ocean circulation. Deep-Sea Res. Oceanogr. Abstr. 9 (1–2), 11–23. https://doi.org/10.1016/0011-7471(62)90243-7.
Yashayaev, I., 2007. Hydrographic changes in the Labrador Sea, 1960–2005. Prog. Oceanogr. 73 (3–4), 242–276. https://doi.org/10.1016/j.pocean.2007.04.015.
Zeebe, R.E., Wolf-Gladrow, D.A., 2001. CO_2 in Seawater: Equilibrium, Kinetics, Isotopes. Elsevier, Amsterdam.